Copy 6
RM L54K17

RESEARCH MEMORANDUM

RESULTS OF INITIAL WIND-TUNNEL FLUTTER EXPERIMENTS AT LOW SPEED WITH A TOWED AIRPLANE MODEL HAVING A 40° SWEPTBACK WING OF ASPECT RATIO 3.62 EQUIPPED WITH PYLON-MOUNTED STORES

By Albert P. Martina and George E. Young

Langley Aeronautical Laboratory
Langley Field, Va.

NATIONAL ADVISORY COMMITTEE
FOR AERONAUTICS

WASHINGTON
March 24, 1955

NATIONAL ADVISORY COMMITTEE FOR AERONAUTICS

RESEARCH MEMORANDUM

RESULTS OF INITIAL WIND-TUNNEL FLUTTER EXPERIMENTS AT LOW SPEED WITH A TOWED AIRPLANE MODEL HAVING A 40° SWEPTBACK WING OF ASPECT RATIO 3.62 EQUIPPED WITH PYLON-MOUNTED STORES

By Albert P. Martina and George E. Young

SUMMARY

Wind-tunnel flutter tests at Mach numbers from 0.14 to 0.24 have been conducted on a swept-wing towed airplane model equipped with an autopilot system. The towed-airplane-model technique permits the model to fly in the wind tunnel with all of the body freedoms except longitudinal translation. All of the model components except the wing were of essentially rigid construction. The wing was of NACA 64A-series airfoil sections having a streamwise thickness of 7.7 percent. The wing aspect ratio was 3.62 and was of spar-pod type construction. Pylon-mounted external stores housed flutter-damping devices. The onset of flutter did not appear to affect the flight behavior of the model appreciably. The model experienced wing flutter in a symmetrical mode. Body motions attributable to flutter were small to negligible. The additional freedoms allowed by the towed model altered the flutter speeds by from 5 percent below to 10 percent above the corresponding fixed-root conditions depending on the store mass parameters. For the range investigated the store moments of inertia had a large influence on the flutter speeds, whereas changes in the store centers of gravity had small or no influence.

INTRODUCTION

Until recently, experimental wind-tunnel flutter research directed toward the determination of flutter characteristics with fuselage mobilities (refs. 1 to 6) paralleled theoretical assumptions in that only the degrees of freedom which were believed to be pertinent to the type of flutter being studied were allowed, whether symmetrical or antisymmetrical. However, after spending considerable effort on

limited freedom techniques, the work of the Boeing Airplane Co. (ref. 6) indicated that a satisfactory test technique should simultaneously allow nearly all of the degrees of freedom of the full-scale counterpart in order to simulate accurately the interaction of the various airplane components resulting from fuselage mobilities. A technique was consequently developed (ref. 6) which allowed four of the six freedoms with elastic restraints in the remaining two, that is, longitudinal and side translation.

In an effort to advance the progress toward the development of wind-tunnel flutter test techniques with still more body freedoms and which have possibilities of being used in the transonic regime, the National Advisory Committee for Aeronautics has embarked on a program to develop the towed-airplane-model test technique in which all of the degrees of freedom except longitudinal translation are provided.

The model used in this development had a 40° sweptback wing of aspect ratio 3.62 and was representative of current fighter-airplane design practices. Two sets of wing panels were constructed; one set was made rigid enough to insure freedom from flutter within the speed range of these tests and was used in the stability and control development phase (ref. 7), whereas the second set was made flexible enough to flutter in the speed range of these tests. All of the other components such as fuselage, control surfaces, control linkages, and external-store pylon mounts were made essentially rigid. The model was controlled by an autopilot system and was protected against divergent flutter motion (when fitted with flexible wings) by flutter-stopping devices housed in the external stores.

After satisfactory stability and control was developed with the rigid wings (ref. 7), the flexible wings were installed and an investigation concerning the effects of variations in the external-store mass parameters on the flutter characteristics was undertaken. Inadvertent loss of the model for reasons not associated with flutter occurred before completion of the investigation, but enough data had been obtained to permit some observations to be made. The present report presents these results, as well as some results of varying the autopilot response. A few flutter tests of each of the flexible wing panels with the root rigidly mounted on a reflection plane had also been made so that some indication of the effects of fuselage mobility is presented. The tests were conducted in the Langley 19-foot pressure tunnel at Mach numbers and Reynolds numbers varying from 0.15 to 0.25 and 1.6×10^6 to 2.8×10^6, respectively. Flutter speeds calculated by means of the method of reference 8 are also presented.

[redacted]

SYMBOLS

The model axes system has its origin at the model center of gravity (located in the model plane of symmetry) with the X-axis parallel to the fuselage center line and the Y-axis perpendicular to the model plane of symmetry.

EI	flexural rigidity of wing section, lb-in.^{2}
GJ	torsional rigidity of wing section, lb-in.^{2}
I_X, I_Y, I_Z	moment of inertia of model about respective model axes, lb-in.^{2}
I_{Y_S}	moment of inertia of external store about an axis coincident with the elastic axis at the point of store attachment to the wing and parallel to the Y-axis, lb-in.^{2}
I_α	polar moment of inertia of wing per unit length about spar axis, lb-in.^{2}/in.
$K_{\theta'}$	elevator-position control-gearing ratio, δ_e/θ'
$K_{\dot{\theta}}$	pitch-damper gearing ratio, $\delta_e/\dot{\theta}$
K_φ	roll-autopilot gearing ratio, δ_a/φ
$K_{\psi'}$	rudder-position control-gearing ratio, δ_r/ψ'
$K_{\dot{\psi}}$	yaw-damper gearing ratio, $\delta_r/\dot{\psi}$
M	Mach number
R	Reynolds number
V	velocity, mph
V_f	experimental flutter speed, mph
W	weight of model, lb
W_W	weight of one wing panel, lb
W_S	weight of external store and pylon, lb

[redacted]

c	wing chord parallel to airstream, in.
$\bar{c}$	wing mean aerodynamic chord, in.
c'	wing chord normal to spar axis, in.
f_f	flutter frequency, cps
f_n	experimental frequency of vibration of wing in the nth natural mode, cps
g	total damping coefficient, $\frac{1}{n\pi} \log_e \frac{\text{Amplitude at 0 cycles}}{\text{Amplitude at n cycles}}$
l	length of wing along spar axis, in.
l'	length of external store, in.
w	weight of wing per unit length, lb/in.
$x_{E.A.}$	location of wing spar axis from leading edge, positive rearward, in.
$\bar{x}$	location of model center of gravity measured from leading edge of mean aerodynamic chord, positive rearward, in.
$\bar{x}_n$	location of external-store center of gravity measured from nose of store, in.
$\bar{x}_s$	location of external-store center of gravity measured from nose of wing section at spanwise location of store, positive rearward, in.
$\bar{x}_o$	location of center of gravity of wing section from leading edge of section, positive rearward, in.
$\bar{x}_{o'}$	location of center of gravity of wing section from leading edge of section in a plane normal to the spar axis, in.
y'	distance along spar axis from model center line, positive toward tip, in.
$\bar{z}$	vertical location of model center of gravity from fuselage reference line, positive upwards, in.
$\bar{z}_s$	vertical location of external-store center of gravity measured from spar axis parallel to Z-axis, positive upwards, in.

[redacted]

δ_a	total (left plus right) aileron deflection perpendicular to aileron hinge line, positive to produce positive roll, radians
δ_e	elevator deflection perpendicular to elevator hinge line, positive trailing edge down, radians
δ_r	rudder deflection perpendicular to rudder hinge line, positive trailing edge left, radians
θ'	angle between a plane parallel to XY-plane and a plane normal to XZ-plane and containing the tow rod, radians
$\dot{\theta}$	pitching angular velocity, radians/sec
ρ	density of air, slugs/ft^3
φ	angle of roll, radians
ψ'	angle between XZ-plane and a plane normal to XY-plane and containing the tow rod, radians
$\dot{\psi}$	yawing angular velocity, radians/sec
ω	angular frequency of vibration, radians/sec
$\frac{\omega\bar{c}}{2V}$	reduced frequency parameter, referred to wing mean aerodynamic chord

MODEL

The model used in this investigation was representative of current fighter-airplane design practices both in regard to geometric configuration and to dynamic characteristics. All the model components except the wings were essentially rigid. Photographs of the model resting on the landing mat are shown in figure 1. Pertinent model dimensions are given on the three-view drawing which is presented in figure 2, and the model mass characteristics are given in table I. The various model configurations are designated by a system of numbers which describe the principal store mass parameters and will be used throughout this report. For example, the configuration "56-25-3.18" has the following connotation:

56	weight of external store in percent of wing-panel weight
25	store center of gravity from leading edge of wing chord at spanwise location of external store in percent chord

[redacted]

3.18 polar moment of inertia in pitch of external store about axis of wing spar at spanwise location of external store in percent of the airplane-model pitching inertia without stores

Moreover, in the case of the towed model, the averages of the left and right external stores are used to describe the configuration. As shown in figure 3, the model was constructed in five major components - the left and right wing panels and three fuselage sections.

Fuselage and Tail

The central or main-fuselage section to which all of the other components were attached was a welded semimonocoque structure of high rigidity fabricated of 1/8-inch-thick magnesium plate. This section housed the roll-control gyro and contained mounting pads for the wing panels and for the wiring terminal blocks. The fuselage contours over this section as well as the fuselage nose and rear sections were formed of molded sections having surfaces of fiber-glass laminations impregnated with a thermosetting plastic and bonded to a foamed plastic core approximately 1/4 inch thick. The dorsal and vertical fins were built integral with the rear fuselage section. The tow-rod pivot support was mounted just inside the nose and was located on the fuselage center line as shown in figure 2. The horizontal stabilizer was bolted to integral metal pads in the vertical fin and was of laminated plastic construction. The elevators and rudder were of the unbalanced plain-flap type and were also of laminated plastic construction. All the movable control-surface hinges were equipped with small ball bearings.

The model landing gear was of welded tubular-steel construction incorporating coil-spring shock absorbers.

Wing

The wing was swept back 40° at the quarter-chord line, had an aspect ratio of 3.62, a taper ratio of 0.561, and embodied 3.5° negative dihedral. The airfoils were nominally NACA 64A010 sections normal to the quarter chord. Each wing panel consisted of a duralumin spar to which were attached 12 balsa segments or "pods" which formed the wing surfaces as shown in figure 4(a). The wing spar axis with 37.25° sweepback was straight and was located at 41-percent wing-fuselage-juncture chord and at 38 percent of the tip chord. The pods were bolted to the drag flanges of the spar with thin washer separators between the flanges and the pods as shown in figure 4(b). These washers minimized the restraint of the pods so that the spar rigidities were unaltered by their attachment. The structural properties of the assembled wing panels are

given in figure 5. The bending and torsional rigidities were experimentally determined by measuring the slope and twist distributions of the respective deflection curves obtained from the application of known moments to the wing, whereas the drag stiffness was calculated by using beam theory. All the pods were ballasted with brass slugs resulting in the spanwise variations of mass properties as given in figure 6. The data points are plotted at the spanwise locations of the pod centers of gravity. The section moments of inertia were obtained by experimentally determining the moment of inertia of each of the pods, adding in the calculated spar contributions, and dividing by the pod widths. The measured cantilever vibration frequencies and predominant modes of the wing panels mounted with root fixed and without external stores are given in the following table:

Panel	f_1 first bending	f_2 first torsion	f_3 second bending
Left	6.73	24.0	29.0
Right	6.65	24.2	28.9

The gaps between pods were sealed with thin rubber strips as shown in figure 4(a). Full chord wraparound fences were located at 0.653 semispan and were divided into segments and sealed with thin rubber where the fences crossed from one pod to an adjacent pod as shown in figure 4(d). Rounded tips of light construction were added for the towed-model tests. The ailerons were of the unbalanced plain-flap type and were made of solid balsa with 1/4-inch-diameter steel drill rod spars at the hinge axes. The aileron hinges were equipped with small self-alining ball bearings and were supported by means of brackets as shown in figure 4(a). Details of the mounting of the outer aileron hinge bracket are shown in figure 4(c), and it is pointed out that sufficient clearance was provided around this bracket so that the only point of attachment was at the spar.

Autopilot

Control of the model was effected by means of an autopilot system since it was felt that limited maneuvering distances coupled with the anticipated model frequencies would render manual operation of the controls very erratic. The general arrangement is shown in figure 7 and a detailed description is given in reference 7.

The model ailerons were made to deflect in proportion to the bank angle of the model by a direct coupled electrically driven displacement gyro operating at about 11,000 rpm and housed in the fuselage center section. The gearing ratio between the displacement gyro and the ailerons could be adjusted before a test. A remote electrical control

was used to trim the ailerons to correct for drift of the gyro while in flight. The elevators and the lower half of the rudder were linked to the tow line in such a manner that the control deflections were proportional to the angular movements of the tow line about the tow-rod pivot point and in such a direction as to cause the model to aline itself with the tow line. The tow line was attached to the model through a tow rod at the pivot point shown in figure 2. The tow rod was a 3/8-inch aluminum rod about 38 inches long pinned to a universal-joint arrangement which allowed the rod to have any combination of yaw and pitch angles with respect to the model. The function of the tow rod was to provide moments sufficiently large to overcome the hinge moments arising from the aerodynamic forces on the control surfaces and from control linkage friction. The gearing ratios between the tow line and the various control surfaces could be adjusted before a test. A remotely operated trim control was provided for the elevators so that the model vertical position in the tunnel could be controlled in flight. All the control linkages, pivot supports, and the like were ball-bearing equipped

The upper half of the rudder was used as a yaw damper in order to reduce a Dutch roll oscillation to a tolerable level. This portion of the rudder was linked to a servomotor which was energized in proportion to the yawing angular velocity as measured by a small air-driven rate gyro, with the rate-gain factor being controllable in flight.

For those tests in which a pitch damper was used, each elevator was divided into two parts with the outer halves used with the damper. The damper was actuated in a manner similar to that of the yaw damper except that the pitch-damper gyro was oriented to measure the pitching angular velocity.

External Stores

The external stores were pylon-mounted at 71.3-percent semispan as shown in figure 2. The stores were constructed in three sections as shown in figure 3: a duralumin center section and a plastic-impregnated laminated fiber-glass forebody and afterbody. The external-store ordinates are given in table II. The store mass parameters were varied by changing the positions of lead or brass weights in the forebody and afterbody. Table III gives the values of the various external-store mass parameters which were tested. The center sections of the stores were mounted to the wing by means of duralumin pylons having rectangular sections as shown in figure 8 and were enclosed in a wood-plastic-impregnated fiber-glass pylon fairing. As seen in the figure, the pylons were mounted onto the drag flanges of the spars with thin washer separators between the mounting pads and the spar flanges, a mounting which did not appreciably alter the spar rigidities. Loss of the model prevented the experimental determination of the frequencies of vibration

[redacted]

of the pylon-store combinations as mounted on the wing for the various configurations tested. The calculated pylon-store frequencies, however, are presented in table IV for the various configurations. In these calculations the pylon mount at the spar was assumed built in and it is seen that the lowest frequencies are well outside of the flutter-frequency ranges. The frequencies and modes of natural vibration for the wing panels in combination with the various external-store configurations are given in tables V and VI.

Flutter Stoppers

Small air-driven gyroscopes having their axes of spin parallel to the direction of air flow were mounted to the store center sections and served as flutter stoppers. The application of gyroscopes in these tests was a modification of the principle demonstrated in the Survey Course in Aeroelasticity conducted at the Massachusetts Institute of Technology in July 1952 in which gyroscope dampers were used to raise the flutter speeds of a wind-tunnel model. As seen in the schematic representation of figure 9, the gyroscope (1) was mounted in the inner gimbal (2) which was restrained about the precession axis B-B by the damper (7). The inner gimbal was mounted to the outer gimbal (3) which was normally free to rotate about the axis C-C in the frame (4) attached to the external store. The axis C-C was parallel to the Y or pitch axis. When the stopper was called upon to stop flutter, the locking pinion (6) was caused to contact the sector gear (5) and thus restrain the outer gimbal from rotation with respect to the frame. The gyro was thus coupled to the wing and subjected to the angular velocity produced by the wing torsional motion during flutter. The gyroscope then would precess about the axis B-B opposed by the action of the viscous damper. This, in effect, added to the wing torsional damping which raised the flutter speeds in these tests. The fluid used was a silicone compound having a viscosity of 1×10^6 centistokes and which varied but little over a wide temperature range. As would be expected, it was found that the gap between the damper discs was very critical in obtaining the maximum damping of the torsional mode; a gap of 0.020-inch width was used for these tests. The torsional damping coefficients measured at zero airspeed with the dampers energized were 0.14, or about six times greater than the wing damping coefficients.

The cross section through the store shown in figure 8 illustrates the actual setup of the gyroscope and locking pinion. The locking pinion was actuated by an air bellows supplied with high-pressure air through an electrically operated solenoid air valve.

INSTRUMENTATION AND APPARATUS

Towed Model

The bending and torsional strains on the spars were measured by using electrical resistance-type strain gages attached at the stations shown in figure 4(a). The movements of the outer gimbals on the flutter stoppers (③ of fig. 9) were measured by means of differential transformers, the cores of which were linked to the outer gimbals. Three accelerometers were used to record the model motions in pitch, roll, and vertical translation with one accelerometer located at the center of gravity and the other two located laterally and forward of the center of gravity. The model control-surface positions were recorded by means of differential-type transformers linked to each control surface. The electrical leads from all of these units as well as the power leads for the roll-control gyro, various servomotors, and an air-supply line were carried out through the nose of the model and along the tow cable to the support yoke (section B-B, fig. 10), thence along the left-yoke support cable through the tunnel wall to the recording station. All the data were recorded on an 18-channel recording oscillograph.

The outputs of the left and right sets of outboard strain gages were also amplified and fed into a two-beam oscilloscope in order to present an additional picture of the onset of flutter. In this arrangement, the bending outputs were fed into the vertical axes and the torsional outputs were fed into the lateral axes and their magnitudes so amplified that at flutter the dots on the oscilloscope screens traced elliptic Lissajous patterns. In order to provide a means of checking the operation of the flutter stoppers during flight, the outputs of the outer gimbal-position transformers were also fed into two additional oscilloscopes indicating the movement of the gimbals directly.

An automatic tripping device was incorporated in the bending-gage circuits to actuate the recorder in case either of the two observers had failed to take records. Tunnel speeds at flutter were recorded by the tunnel operator who received a light signal indicating when a flutter record was being taken.

Motion-picture cameras located above, abreast, and downstream of the model were used to record the motions of the model during flutter and whenever the situation demanded.

The model tow cable consisted of a 1/16-inch aircraft cable attached to the upstream tunnel guide vanes and was rigidly supported by the yoke (section B-B, fig. 10). The landing mat was supported along its center line on a channel and was constructed of 3/4-inch plywood covered with approximately 1 inch of hard sponge rubber. The

[redacted]

manually operated snubbing wire was used to secure the model firmly to the landing mat during take-offs and landings, but was left completely slack during flight.

Fixed-Root-Test Setup

For the fixed-root tests of each wing panel a reflection plane mounted on the tunnel floor was used as shown in figures 11 and 12. The bending and torsion strains, the model-flutter-stopper position, and the tunnel-flutter-stopper position were recorded in these tests.

The reflection plane was constructed of 3/4-inch plywood attached to the tunnel walls at the edges and to two steel channels running nearly the full length on either side of the tunnel center line. The wing panel was attached to a heavy steel turntable mounted atop the support mount. The mount was fabricated from heavy steel plate and was attached to the rather massive tunnel balance frame.

Inasmuch as the tunnel airspeed could not be reduced very quickly, a retractable tunnel flutter stopper which when ejected provided a localized region of reduced velocity around the model was used in the fixed-root tests. The operating time of this stopper was about 0.7 second. The stopper shown in figure 12(b) consisted of a duralumin frame to which a reinforced 16-mesh screen was attached. Measurements showed that this screen reduced the velocity about 25 percent in the region occupied by the model.

TEST PROCEDURE

The tests were conducted in the Langley 19-foot pressure tunnel at atmospheric pressure. The resulting Mach number and Reynolds number variations with airspeed are presented in figure 13 for the range covered in these tests.

Towed-Model Tests

Before actually beginning a towed-model test it was necessary to start the roll-displacement gyro since several minutes were required for the displacement gyro to attain its operating speed of 11,000 rpm. The flutter-stopper gyros and the yaw-damper gyro were also started and allowed to attain operating speeds of 60,000 rpm and 70,000 rpm, respectively. System checks and check calibrations were also made before each test.

In obtaining a typical towed-model flutter test point the tunnel airspeed was brought up to the take-off speed which for expediency was set at between 100 and 105 mph in these tests. At the take-off speed the snubbing wire was made slack while the flight director (see fig. 10) simultaneously retrimmed the elevators until the model rose to the desired position. As the model rose, the ailerons were retrimmed to correct for the drift of the roll-displacement gyro by an operator who viewed the model through a canopy at the center line of the tunnel floor. (See fig. 10.) After steady flight conditions were established the tunnel airspeed was usually increased in 5- or 10-mph steps depending on the proximity to flutter. During speed changes, particularly rapid speed changes, it was oftentimes necessary to halt the speed increases because of large model oscillations arising from air-flow disturbances and to allow the oscillations to damp until steady flight was again established. About 10 to 20 mph below the anticipated flutter speeds, the model flutter stoppers were actuated to ensure the proper functioning of all components. Random tunnel disturbances of an intensity sufficient to excite either or both wing panels occurred frequently enough to give at least a 2- to 3-mph warning of the onset of flutter. As the wing damping appeared to decrease, the tunnel-speed increases were then made in 1-mph steps or less until flutter was obtained. The flutter observer, an observer at the central recording station, or the automatic tripper then turned on the recording equipment which was allowed to record for several seconds before the model flutter stoppers were energized. The tunnel airspeed was then lowered and when sufficiently low the flight director would trim the elevators to allow the model to settle to the landing mat while the snubbing wire was made taut to terminate the test. In order to keep constant checks on the structural integrity of the wing panels, the wing vibration frequencies were measured before and after each test by vibrating the model on its landing gear or on a fuselage-support dolly resting on the landing mat.

At one time during the test program when the flexible wings were removed for repairs to the strain gages, the opportunity was taken to check for any reduction in the panel stiffness distributions to see if there had been any damage.

Fixed-Root Tests

The fixed-root flutter tests were performed in a manner which was generally similar to the towed-model tests except that the flutter observer was located at the top of the tunnel (see fig. 11) and controlled both the tunnel and model flutter stoppers. The ailerons were secured in their neutral position with cellulose tape for these tests.

No corrections to the fixed-root flutter speeds were made for the boundary layer on the reflection plane inasmuch as measurements made in

the region occupied by the wing panels indicated that the thickness of the boundary layer was only 6 percent of the semispan and that the average airspeed was about 99 percent of the average tunnel airspeed. It is believed that the dropoff in velocity in the localized root region would have little effect on the wing flutter speeds.

RESULTS AND DISCUSSION

Towed Model Tests

Flutter characteristics.- The flutter characteristics of the towed model are given in table V and in figure 14. Portions of oscillograms made during a typical flutter test are shown in figure 15 for velocities of 95.5, 97.8, and 100 percent of the flutter velocity. As seen in figure 14, the flutter speeds for the towed model were lowered as the store inertias were increased. With a store weight of 56 percent of the wing weight, a linear variation of flutter speed with increasing store inertia ratio was obtained for the store centers of gravity at 25 percent wing chord. Moving the store centers of gravity rearward from 25 to 32 percent chord had little effect on the flutter speeds at the higher store inertias but effected progressively larger reductions as the store inertias were decreased. The changes due to moving the store centers of gravity displayed the same trends as reported in reference 9. The dotted portion of the curve represents an extrapolation made on the basis of the maximum speed of 175.3 mph experienced for the 56-25-1.91 configuration. The model was subsequently destroyed at this speed as a result of a power failure to the autopilot. The oscillograph had been recording for over 2 seconds prior to the crash and these records indicated that the model was experiencing incipient flutter. Inasmuch as the frequencies f_2 were nearly proportional to the store inertias I_{Y_S}, the flutter speeds decreased nearly in proportion to the increase in the frequency ratios f_1/f_2 as seen in table V.

The flutter modes appeared to be of the symmetric bending-torsion type, with the torsion component very prominent in all cases. The flutter motions appeared to be of a mild, very slowly diverging nature; however, the motions tended to become somewhat more explosive at the higher airspeeds. The flutter motions were allowed to reach amplitudes at the tips which varied from approximately 1/4 to 3/4 inch in bending and two to three degrees in torsion. These amplitudes were based on the results of static strain calibrations.

The onset of flutter did not appear to affect the flight behavior of the model appreciably at any speed. The short-period lateral and longitudinal oscillations were between 1 and 2 cycles per second varying slightly with airspeed. The average amplitudes of the rolling oscillations were from 5° to 6° at the lower speeds and 7° to 8° at the higher speeds and appeared to be unaffected by the onset of flutter although

increased autopilot activity was noted at flutter. It was observed on several occasions that, when the flutter dampers were actuated at flutter, the rolling oscillations were momentarily reduced to about half the normal values but that the oscillations quickly increased in amplitude to their normal values.

The model flew smoothly up to 160 mph and in this speed range slight pitching and very small vertical translation were occasionally observed at flutter for some of the configurations. Elevator motions as large as $\pm 1^{\circ}$ accompanied the body motions. The extent to which the tow-line inertia influenced these motions is currently unknown; although in view of the observed reflection of tow-line disturbances from the tow-line support point, it is suspected that conditions could exist in which the tow line would have a large influence on the motions.

Above a tunnel airspeed of 160 mph the model behavior was very "choppy" and was characterized by large displacements. Wing response became noticeable as early as 170 mph for the 33-24-1.14 configuration with frequent bursts of flutter setting in at 180 mph. It is not certain whether a noticeable change in the tunnel air flow occurred in this speed range since neither tunnel frequency nor amplitude spectra are available. At flutter, the pitching motions at these higher speeds as indicated by the accelerometer records were barely perceptible, whereas the elevator motions were negligible.

Considerations on the effects of the autopilot.- Some concern was felt as to the possible aerodynamic effects of the operating ailerons on the flutter characteristics of the flexible wings since all of the flutter tests on the towed model were necessarily made with the autopilot system operative, and increased roll autopilot activity was noted at flutter. Consequently, the flutter characteristics of the towed model with flexible wings were determined for a range of roll-gearing ratios at both extremes of the speed range, that is, 110 and 185 mph. (See table V.) The ranges of gearing ratios which could be safely flown as well as the test results are summarized below:

Configuration	K_{φ}	V_f
56-25-3.18	2.0:1	109.5
56-25-3.18B	2.6:1	110.5
56-25-3.18C	3.0:1	111.2
33-24-1.14A	2.6:1	185.9
33-24-1.14D	2.0:1	191.0

[redacted]

It is seen that the maximum variations in the flutter speeds occurred at the higher speeds and were less than 3 percent. Thus, it is concluded that, for the range of roll-gearing ratios that could be tested, the effects of the changes in the roll autopilot sensitivity on the flutter characteristics were minor since the maximum variation in flutter speeds was believed to approach the repeatability of a given test point. The repeatability from two trials made in separate tests (table V, configurations 33-24-1.14C and 33-24-1.14D) was believed to be about 2 percent. The change in $K_{\dot{\psi}}$ between these cases was believed to be unimportant. It is of interest to note in table V that for the 56-25-3.18 configuration the changes in the pitch autopilot parameters had negligible effect on the flutter characteristics (comparing 56-25-3.18A with 56-25-3.18B). The small change in $K_{\dot{\psi}}$ between these two tests was believed to be insignificant. It had been previously determined during tests with the rigid wings that the towed-model flight behavior was relatively insensitive to changes in the pitch-displacement control-gearing ratios.

Thus, for the range of autopilot gearing ratios which could be flown safely, it is believed that the effects on flutter of varying the autopilot restraints were second order as regards the trends and characteristics presented. However, it should not be construed from these meager results that the effects of the controls will always be small. Each case will probably have to be investigated separately.

Fixed-Root Tests

Preliminary to the tests of the towed model a few fixed-root tests were made to determine the flutter speeds of each wing panel and to check the performance of the flutter dampers. These were the only fixed-root results which were made because the subsequent destruction of the towed model prevented the completion of those fixed-root tests which were to have followed the towed-model tests.

The pertinent results of the fixed-root tests are presented in table VI. The initial tests for the 56-25-3.18 configuration indicated that the left panel fluttered about 5 mph before the right wing. Near identical flutter speeds were obtained by adjusting the left store inertia downward. The flutter motions in the fixed-root tests were allowed to reach bending amplitudes at the tips of from 1/2 to 1 inch and torsional amplitudes of about 3° to 4°.

Comparison Between the Towed-Model and Fixed-Root Tests

The fixed-root results are compared with those of the towed model in figure 14. It can be seen that the additional body freedoms provided

by the towed model altered the flutter speeds from 5 percent below to 10 percent above the corresponding fixed-root conditions, depending on the store mass parameters. The towed-model flutter frequencies on the other hand were all from 5 to 8 percent higher than the corresponding fixed-root flutter frequencies.

It is of interest to note that, in several instances, both during the fixed-root tests and during flight tests when the tunnel airspeed was maintained after energizing the flutter dampers, the original bending-torsion flutter was damped for several seconds, but that flutter again set in at somewhat lower frequencies. The frequencies were nearer to the bending frequencies, about 1 cycle per second less than the original flutter frequencies, and there appeared to be very little torsion component in the motions. The bending amplitudes were considerably less than the bending components during undamped flutter. No obvious explanation is apparent other than the possibility of a change in the characteristics of the damping fluid caused by prolonged motion of the flutter dampers.

Comparison Between the Calculated and Experimental Flutter Characteristics

The calculated flutter characteristics for the towed model (fig. 16) agreed reasonably well with experiment except for those cases in which the store loadings were 56 percent of the wing weight and had the centers of gravity at 25 percent chord. The calculated trends for these 56-25-xxx cases were opposite those found experimentally. The calculations, based on the method described in appendix A, were made by using two elastic modes: first uncoupled bending and torsion, and rigid-body vertical translation and pitch. The store pylons were assumed to be rigid and the store aerodynamics were neglected. The swept-wing aerodynamics of reference 8 with the lengthwise flow terms neglected were used in the calculations. No aspect-ratio or compressibility corrections were used.

The calculated flutter characteristics for the wing panels with root fixed (fig. 17) agreed reasonably well with experiment except for the flutter speed at the highest inertia forward center-of-gravity loading. The same assumptions were made as in the towed-model calculations except, of course, for the neglect of the body translation and pitch freedoms.

The disagreement between the calculations and experiment for those cases having high mass coupling (forward-store center of gravity and high-store inertia) follows the trend found with unswept wings in references 10 and 11, with the disagreement progressively becoming

greater with increased mass coupling. It is believed that the inclusion of more elastic wing modes would probably improve the agreement between the calculated and experimental characteristics for the highly mass-coupled cases.

The calculated incremental effects on the flutter speeds of the additional freedoms allowed by the towed model agreed fairly well with the experimental effects with the exception of the 56-25-3.18 case as shown in the following table:

Configuration	$V_{f_{towed\ model}}/V_{f_{fixed\ root}}$	
	Calculated	Experimental
56-25-3.18	≈ 4	0.91 to 0.92
56-33-2.03	1.09	1.06
33-24-1.14	1.04 to 1.06	1.04

SUMMARY OF RESULTS

Initial low-speed tests made in conjunction with the development of a wind-tunnel flutter test technique which permits all of the body freedoms except longitudinal translation and which utilized an auto-pilot-controlled towed airplane model of high rigidity equipped with flexible wings and having external stores indicated the following results:

1. The wing flutter experienced in these tests was of the symmetric bending-torsion type. Body motions in vertical translation and in pitch attributable to flutter were small at the lower speeds and diminished almost entirely at the higher speeds.

2. The additional freedoms allowed by the towed model altered the flutter speeds from 5 percent below to 10 percent above the fixed-root conditions depending on the store mass parameters. The flutter frequencies were from 5 to 8 percent higher than the corresponding fixed-root frequencies.

3. Within the range of this investigation the flutter speeds were not greatly influenced by variations in the external-store centers of gravity, but were critically dependent on the store moments of inertia.

4. The calculated flutter characteristics using the first uncoupled bending and torsion modes for the fixed-root cases plus rigid-body pitch

and vertical translation for the towed-model cases showed good agreement with experiment in many of the cases.

Langley Aeronautical Laboratory,
National Advisory Committee for Aeronautics,
Langley Field, Va., November 12, 1954.

APPENDIX A

FLUTTER-CALCULATION PROCEDURE

The analysis in this paper is of the Rayleigh-Ritz type. The symbols are defined in appendix B. It is assumed that the flutter mode can be represented by a combination of the following four modes:

$\left[Fh_1(\eta)\right] h_1 e^{i\omega t}$	first uncoupled cantilever bending; the mode shape $Fh_1(\eta)$ is that of a tapered beam with the wing weight distribution plus the store weight taken as a concentrated mass
$\left[F\alpha_1(\eta)\right] \alpha_1 e^{i\omega t}$	first uncoupled cantilever torsion; the mode shape $F\alpha_1(\eta)$ is that of a tapered beam with the wing weight distribution plus the store weight taken as a concentrated mass
$h_o e^{i\omega t}$	rigid-body vertical translation
$\theta_o e^{i\omega t}$	rigid-body pitch about airplane center of gravity
$h_1, \alpha_1, h_o, \theta_o$	complex quantities, in general, signifying phase and magnitude relations of the degrees of freedom

The displacements of a mass on the wing due to displacements in these four degrees of freedom are

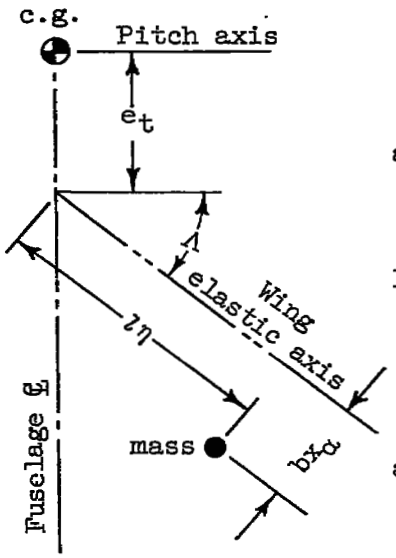

$$h_{mass} = h_o + \left(Fh_1\right)h_1 + bx_\alpha\left(F\alpha_1\right)\alpha_1 + \left(e_t + l\eta \sin \Lambda + bx_\alpha \cos \Lambda\right)\theta_o \quad \text{(A1a)}$$

and

$$\alpha_{mass} = \left(F\alpha_1\right)\alpha_1 + \theta_o \cos \Lambda \quad \text{(A1b)}$$

For the aerodynamic terms,

$$h_{elastic\ axis} = h_o + \left(Fh_1\right)h_1 + \left(e_t + l\eta \sin \Lambda\right)\theta_o \quad \text{(A2)}$$

and

$$\alpha = \left(F\alpha_1\right)\alpha_1 + \theta_o \cos \Lambda$$

[redacted]

The general equation of equilibrium for each degree of freedom, by using Lagrange's equation, is

$$\frac{d}{dt}\frac{\partial T}{\partial \dot{q}_i} - \frac{\partial T}{\partial q_i} + \frac{\partial U}{\partial q_i} = Q_i \tag{A3}$$

where T and U represent, respectively, the total kinetic and potential energy of the airplane, Q_i represents the generalized aerodynamic and structural damping forces in the ith degree of freedom, and q_i is the generalized coordinate.

The swept-wing aerodynamics developed in reference 8 are used except for those due to lengthwise flow. Applying equation (A3) in a manner similar to reference 8, together with some algebraic manipulation, results in the following equations of equilibrium:

$$\left.\begin{aligned}
\pi\rho b_r^3\omega^2 l\left(A_{11}\frac{h_1}{b_r} + B_{11}\alpha_1 + A_{1h_o}\frac{h_o}{b_r} + B_{1\theta_o}\theta_o\right) &= 0 \\
\pi\rho b_r^4\omega^2 l\left(D_{11}\frac{h_1}{b_r} + E_{11}\alpha_1 + D_{1h_o}\frac{h_o}{b_r} + E_{1\theta_o}\theta_o\right) &= 0 \\
\pi\rho b_r^3\omega^2 l\left(A_{h_o1}\frac{h_1}{b_r} + B_{h_o1}\alpha_1 + A_{h_oh_o}\frac{h_o}{b_r} + B_{h_o\theta_o}\theta_o\right) &= 0 \\
\pi\rho b_r^4\omega^2 l\left(D_{\theta_o1}\frac{h_1}{b_r} + E_{\theta_o1}\alpha_1 + D_{\theta_oh_o}\frac{h_o}{b_r} + E_{\theta_o\theta_o}\theta_o\right) &= 0
\end{aligned}\right\} \tag{A4}$$

The solution of this set of homogeneous equations, other than the trivial one in which all the coordinates are zero, is found by equating the determinant of the coefficients to zero. The resulting stability equation gives the conditions for neutrally stable oscillations.

The foregoing analysis may be extended to include more elastic modes by merely adding the modes to equations (A1) and (A2). The flutter determinant for the general case may be written for R bending modes and S torsion modes as follows:

$$\begin{vmatrix}
A_{ij} & B_{ij} & A_{ih_o} & B_{i\theta_o} \\
D_{ij} & E_{ij} & D_{ih_o} & E_{i\theta_o} \\
A_{h_oj} & B_{h_oj} & A_{h_oh_o} & B_{h_o\theta_o} \\
D_{\theta_oj} & E_{\theta_oj} & D_{\theta_oh_o} & E_{\theta_o\theta_o}
\end{vmatrix} = 0$$

[redacted]

where

$$A_{ij} = -\int_0^1 B^2 A_{ch}\left[Fh_i(\eta)\right]\left[Fh_j(\eta)\right]d\eta + \lambda\int_0^1 B^3 \frac{i}{k_n} A_{ch}\left[Fh_i(\eta)\right]\frac{d}{d\eta}\left[Fh_j(\eta)\right]d\eta \qquad (i \neq j) \quad \begin{matrix} i = 1,2,3, \ldots R \\ j = 1,2,3, \ldots R \end{matrix}$$

$$A_{ii} = \int_0^1 B^2\left[\frac{1}{\kappa}\left(1 - \omega_{h_i}{}^2\Omega_i\right) - A_{ch}\right]\left[Fh_i(\eta)\right]^2 d\eta + \lambda\int_0^1 B^3 \frac{i}{k_n} A_{ch}\left[Fh_i(\eta)\right]\frac{d}{d\eta}\left[Fh_i(\eta)\right]d\eta$$

For the diagonal element in the ith bending mode,

$$B_{ij} = \int_0^1 B^3\left[\frac{x_\alpha}{\kappa} - A_{c\alpha}\right]\left[Fh_i(\eta)\right]\left[F\alpha_j(\eta)\right]d\eta - \lambda\int_0^1 B^4 A_{cT}\left[Fh_i(\eta)\right]\frac{d}{d\eta}\left[F\alpha_j(\eta)\right]d\eta \qquad \begin{matrix} i = 1,2,3, \ldots R \\ j = 1,2,3, \ldots S \end{matrix}$$

$$A_{ih_o} = \int_0^1 B^2\left[\frac{1}{\kappa} - A_{ch}\right]\left[Fh_i(\eta)\right]d\eta \qquad i = 1,2,3, \ldots R$$

$$B_{i\theta_o} = \frac{e_t}{b_r}\int_0^1 B^2\left[\frac{1}{\kappa} - A_{ch}\right]\left[Fh_i(\eta)\right]d\eta + \gamma\int_0^1 B^2\left[\frac{1}{\kappa} - A_{ch}\right]\left[Fh_i(\eta)\right]\eta\, d\eta + \cos\Lambda\int_0^1 B^3\left[\frac{x_\alpha}{\kappa} - A_{c\alpha}\right]\left[Fh_i(\eta)\right]d\eta + \sin\Lambda\tan\Lambda\int_0^1 B^3\frac{i}{k_n}A_{ch}\left[Fh_i(\eta)\right]d\eta \qquad i = 1,2,3, \ldots R$$

[redacted]

$$D_{ij} = \int_0^1 B^3 \left[\frac{x_\alpha}{\kappa} - A_{ah}\right]\left[F\alpha_i(\eta)\right]\left[Fh_j(\eta)\right] d\eta +$$

$$\lambda \int_0^1 B^4 \frac{i}{k_n} A_{ah}\left[F\alpha_i(\eta)\right]\frac{d}{d\eta}\left[Fh_j(\eta)\right] d\eta \qquad \begin{matrix} i = 1,2,3, \ldots S \\ j = 1,2,3, \ldots R \end{matrix}$$

$$E_{ij} = -\int_0^1 B^4 A_{a\alpha}\left[F\alpha_i(\eta)\right]\left[F\alpha_j(\eta)\right] d\eta -$$

$$\lambda \int_0^1 B^5 A_{ar}\left[F\alpha_i(\eta)\right]\frac{d}{d\eta}\left[F\alpha_j(\eta)\right] d\eta$$

$$(i \neq j) \qquad \begin{matrix} i = 1,2,3, \ldots S \\ j = 1,2,3, \ldots S \end{matrix}$$

$$E_{ii} = \int_0^1 B^4 \left[\frac{r_\alpha^2}{\kappa}\left(1 - \omega_{\alpha_i}{}^2\Omega_i\right) - A_{a\alpha}\right]\left[F\alpha_i(\eta)\right]^2 d\eta -$$

$$\lambda \int_0^1 B^5 A_{ar}\left[F\alpha_i(\eta)\right]\frac{d}{d\eta}\left[F\alpha_i(\eta)\right] d\eta$$

For the diagonal element in the ith torsion mode,

$$D_{ih_o} = \int_0^1 B^3 \left[\frac{x_\alpha}{\kappa} - A_{ah}\right]\left[F\alpha_i(\eta)\right] d\eta \qquad i = 1,2,3, \ldots S$$

$$E_{i\theta_o} = \frac{e_t}{b_r}\int_0^1 B^3 \left[\frac{x_\alpha}{\kappa} - A_{ah}\right]\left[F\alpha_i(\eta)\right] d\eta + \gamma \int_0^1 B^3 \left[\frac{x_\alpha}{\kappa} - A_{ah}\right]\left[F\alpha_i(\eta)\right]\eta\, d\eta +$$

$$\cos\Lambda \int_0^1 B^4 \left[\frac{r_\alpha^2}{\kappa} - A_{a\alpha}\right]\left[F\alpha_i(\eta)\right] d\eta +$$

$$\sin\Lambda \tan\Lambda \int_0^1 B^4 \frac{i}{k_n} A_{ah}\left[F\alpha_i(\eta)\right] d\eta \qquad i = 1,2,3, \ldots S$$

[redacted]

$$A_{h_o j} = \int_0^1 B^2\left[\frac{1}{\kappa} - A_{ch}\right]\left[Fh_j(\eta)\right]d\eta +$$

$$\lambda \int_0^1 B^3 \frac{i}{k_n} A_{ch} \frac{d}{d\eta}\left[Fh_j(\eta)\right]d\eta \qquad j = 1,2,3, \ldots R$$

$$B_{h_o j} = \int_0^1 B^3\left[\frac{x_\alpha}{\kappa} - A_{c\alpha}\right]\left[F\alpha_j(\eta)\right]d\eta -$$

$$\lambda \int_0^1 B^4 A_{c\tau} \frac{d}{d\eta}\left[F\alpha_j(\eta)\right]d\eta \qquad j = 1,2,3, \ldots S$$

$$A_{h_o h_o} = \frac{M_T}{\pi\rho b_r^3 l} - \int_0^1 B^2 A_{ch}\, d\eta$$

$$B_{h_o \theta_o} = -\frac{e_t}{b_r}\int_0^1 B^2 A_{ch}\, d\eta - \gamma \int_0^1 B^2 A_{ch}\, \eta\, d\eta -$$

$$\cos\Lambda \int_0^1 B^3 A_{c\alpha}\, d\eta + \sin\Lambda \tan\Lambda \int_0^1 B^3 \frac{i}{k_n} A_{ch}\, d\eta$$

$$D_{\theta_o j} = \cos\Lambda \int_0^1 B^3\left[\frac{x_\alpha}{\kappa} - A_{ah}\right]\left[Fh_j(\eta)\right]d\eta + \frac{e_t}{b_r}\int_0^1 B^2\left[\frac{1}{\kappa} - A_{ch}\right]\left[Fh_j(\eta)\right]d\eta +$$

$$\gamma \int_0^1 B^2\left[\frac{1}{\kappa} - A_{ch}\right]\left[Fh_j(\eta)\right]\eta\, d\eta +$$

$$\lambda \cos\Lambda \int_0^1 B^4 \frac{i}{k_n} A_{ah} \frac{d}{d\eta}\left[Fh_j(\eta)\right]d\eta +$$

$$\frac{e_t}{b_r}\lambda \int_0^1 B^3 \frac{i}{k_n} A_{ch} \frac{d}{d\eta}\left[Fh_j(\eta)\right]d\eta +$$

$$\sin\Lambda \tan\Lambda \int_0^1 B^3 \frac{i}{k_n} A_{ch} \frac{d}{d\eta}\left[Fh_j(\eta)\right]\eta\, d\eta \qquad j = 1,2,3, \ldots R$$

[redacted]

$$E_{\theta_o j} = \cos \Lambda \int_0^1 B^4 \left[\frac{r_\alpha^2}{\kappa} - A_{a\alpha}\right]\left[F\alpha_j(\eta)\right] d\eta +$$

$$\frac{e_t}{b_r} \int_0^1 B^3 \left[\frac{x_\alpha}{\kappa} - A_{c\alpha}\right]\left[F\alpha_j(\eta)\right] d\eta +$$

$$\gamma \int_0^1 B^3 \left[\frac{x_\alpha}{\kappa} - A_{c\alpha}\right]\left[F\alpha_j(\eta)\right] \eta \, d\eta -$$

$$\lambda \cos \Lambda \int_0^1 B^5 A_{a\tau} \frac{d}{d\eta}\left[F\alpha_j(\eta)\right] d\eta -$$

$$\frac{e_t}{b_r} \lambda \int_0^1 B^4 A_{c\tau} \frac{d}{d\eta}\left[F\alpha_j(\eta)\right] d\eta -$$

$$\sin \Lambda \tan \Lambda \int_0^1 B^4 A_{c\tau} \frac{d}{d\eta}\left[F\alpha_j(\eta)\right] \eta \, d\eta$$

$$j = 1,2,3, \ldots S$$

$$D_{\theta_o h_o} = -\cos \Lambda \int_0^1 B^3 A_{ah} \, d\eta - \frac{e_t}{b_r} \int_0^1 B^2 A_{ch} \, d\eta - \gamma \int_0^1 B^2 A_{ch} \, \eta \, d\eta$$

$$E_{\theta_o \theta_o} = \frac{I_{\theta_T}}{\pi \rho b_r^4 l} - \cos^2 \Lambda \int_0^1 B^4 A_{a\alpha} \, d\eta - \frac{e_t}{b_r} \cos \Lambda \int_0^1 B^3 \left[A_{c\alpha} + A_{ah}\right] d\eta -$$

$$\gamma \cos \Lambda \int_0^1 B^3 \left[A_{c\alpha} + A_{ah}\right] \eta \, d\eta + \frac{e_t}{b_r} \sin \Lambda \tan \Lambda \int_0^1 B^3 \frac{i}{k_n} A_{ch} \, d\eta +$$

$$\gamma \sin \Lambda \tan \Lambda \int_0^1 B^3 \frac{i}{k_n} A_{ch} \, \eta \, d\eta + \sin^2 \Lambda \int_0^1 B^4 \frac{i}{k_n} A_{ah} \, d\eta -$$

$$\left(\frac{e_t}{b_r}\right)^2 \int_0^1 B^2 A_{ch} \, d\eta - 2 \frac{e_t}{b_r} \gamma \int_0^1 B^2 A_{ch} \, \eta \, d\eta - \gamma^2 \int_0^1 B^2 A_{ch} \, \eta^2 d\eta$$

[redacted]

where $\Omega_i = \frac{1}{\omega^2}(1 + ig_i)$ is the unknown and contains flutter frequency and damping, $B = b/b_r$, $\lambda = \frac{b_r \tan \Lambda}{l}$, and $\gamma = \frac{l \sin \Lambda}{b_r}$.

The quantities A_{ch}, $A_{c\alpha}$, A_{ah}, $A_{a\alpha}$, $A_{c\tau}$, and $A_{a\tau}$ represent expressions for oscillating lift and moment as defined in reference 8.

The equations for the cantilever case, in which h_o/b_r and θ_o are zero, are equations (A4) with the third and fourth rows and columns removed.

[redacted]

APPENDIX B

SYMBOLS FOR APPENDIX A

$Fh_i(\eta)$	calculated amplitude function of wing in ith bending mode
$F\alpha_i(\eta)$	calculated amplitude function of wing in ith torsion mode
I_α	mass moment of inertia of wing per unit length about elastic axis
I_{θ_T}	pitching moment of inertia of model about model center of gravity
M_T	mass of model
V	free-stream velocity
V_n	component of airstream velocity perpendicular to elastic axis, V cos Λ
b	half-chord of wing measured perpendicular to elastic axis
b_r	half-chord of wing at reference station measured normal to elastic axis
e_t	distance between model center of gravity and intersection of elastic axis and the model center line, positive for center of gravity forward
g_i	structural damping coefficient in ith uncoupled mode
h_o	vertical translation of airplane, positive downward
h_i	bending translation of wing in ith mode, positive downward
k_n	reduced frequency referred to velocity component perpendicular to elastic axis, $\omega b/V$
l	length of wing measured along elastic axis from plane of symmetry
m	mass of wing per unit length along elastic axis

[redacted]

r_α nondimensional radius of gyration of wing per unit length about elastic axis, $\sqrt{\frac{I_\alpha}{mb^2}}$

x_α nondimensional location of center of gravity, relative to midchord, from elastic axis measured perpendicular to elastic axis

y coordinate along elastic axis

Λ angle of sweep of elastic axis, deg

α twist of wing about elastic axis, radians

η nondimensional coordinate along elastic axis, y/l

θ airplane pitch, radians

κ mass-density ratio, $\pi\rho b^2/m$

ρ density of air

ω_{α_i} calculated first uncoupled torsional frequency of wing plus store, radians/sec

ω_{h_i} calculated first uncoupled bending frequency of wing plus store, radians/sec

[redacted]

REFERENCES

1. Lambourne, N. C.: An Experimental Investigation on the Flutter Characteristics of a Model Flying Wing. R. & M. No. 2626, British A.R.C., 1952.

2. Broadbent, E. G.: Flutter Problems of High Speed Aircraft. Rep. No. Structures 37, British R.A.E., Apr. 1949.

3. Jordan, P. F., and Smith, F.: A Wind Tunnel Technique for Flutter Investigations on Swept Wings With Body Freedoms. Rep. No. Structures 73, British R.A.E., Sept. 1950.

4. Gaukroger, D. R., Chapple, E. W., and Milln, A.: Wind Tunnel Flutter Tests on a Model Delta Wing Under Fixed and Free Root Conditions. Rep. No. Structures 89, British R.A.E., Sept. 1950.

5. Gaukroger, D. R.: Wind Tunnel Tests on Symmetric Flutter of Swept-Back Wings, Including the Tailplane Effect. Rep. No. Structures 123, British R.A.E., Apr. 1952.

6. Kinnaman, E. Berkeley: Flutter Analysis of Complex Airplanes by Experimental Methods. Jour. Aero. Sci., vol. 19, no. 9, Sept. 1952, pp. 577-584.

7. Schneider, William C.: Development of a New Flutter Testing Technique Using a Towed Dynamic Airplane Model Equipped With an Automatic Stabilizing System - Experimental and Calculated Dynamic Stability Characteristics for Speeds Up to 200 MPH. NACA RM L54L23, 1955.

8. Barmby, J. G., Cunningham, H. J., and Garrick, I. E.: Study of Effects of Sweep on the Flutter of Cantilever Wings. NACA Rep. 1014, 1951. (Supersedes NACA TN 2121.)

9. Gaukroger, D. R.: Wind Tunnel Tests on the Effect of a Localised Mass on the Flutter of a Sweptback Wing With Fixed Root. Rep. No. Structures 159, British R.A.E., Dec. 1953.

10. Woolston, Donald S., and Runyan, Harry L.: Appraisal of Method of Flutter Analysis Based on Chosen Modes by Comparison With Experiment for Cases of Large Mass Coupling. NACA TN 1902, 1949.

11. Runyan, Harry L., and Watkins, Charles E.: Flutter of a Uniform Wing With an Arbitrarily Placed Mass According to a Differential-Equation Analysis and a Comparison With Experiment. NACA Rep. 966, 1950. (Supersedes NACA TN 1848.)

[redacted]

TABLE I

TOWED-MODEL MASS PARAMETERS

Store Configuration (a)	W, lb	$\bar{x}/\bar{c}$	$\bar{z}/\bar{c}$	I_X, lb-in.^{2}	I_Y	I_Z
56-25-3.18	104.5	0.253	-0.066	21,850	30,770	49,710
56-32-2.74	104.5	.263	-.065	21,830	30,850	49,560
56-25-2.72	104.5	.253	-.066	21,860	30,490	49,790
56-32-2.40	104.5	.263	-.065	21,830	30,390	48,600
56-25-2.30	104.5	.253	-.066	21,860	30,270	49,230
56-33-2.03	104.6	.264	-.065	21,850	30,480	49,530
56-25-1.91	104.5	.253	-.066	21,860	29,950	48,910
33-24-1.14	97.8	.216	-.043	17,800	29,800	44,500
Without stores	88.2	.183	-.026	11,350	28,270	37,300

[a]Store configurations are designated as follows: The first number represents W_S/W_W, the second number represents $\bar{x}_s/c$, and the third number represents $\left(I_{Y_S}\right)_{av}/I_{Y_{\text{without stores}}}$.

[redacted]

TABLE II

EXTERNAL-STORE ORDINATES

[Fraction of store length]

Station from nose	Radius
0.0288	0.0249
.0577	.0342
.0865	.0408
.1159	.0456
.1438	.0495
.1727	.0526
.2015	.0547
.2303	.0565
.2589	.0571
.6456	.0571
.6637	.0553
.6997	.0523
.7327	.0486
.7658	.0444
.7988	.0396
.8318	.0345
.8679	.0288
.9009	.0234
.9339	.0156
1.0000	0
Nose radius, 0.015	

[redacted]

TABLE III

EXTERNAL-STORE MASS PARAMETERS

Configuration	Store	W_S, lb	I_{Y_S}	$\bar{x}_S/c$	$\bar{z}_S/c$	$\bar{x}_n/l'$
56-25-3.18	Left	8.15	886.8	0.250	-0.289	0.520
	Right	8.17	909.8	.248	-.289	.518
56-32-2.74	Left	8.17	773.3	.323	-.281	.557
	Right	8.17	773.5	.324	-.281	.558
56-25-2.72	Left	8.17	769.5	.249	-.289	.519
	Right	8.17	771.0	.248	-.289	.519
56-32-2.40	Left	8.17	677.1	.324	-.281	.557
	Right	8.17	678.3	.323	-.281	.557
56-25-2.30	Left	8.17	646.8	.253	-.288	.520
	Right	8.17	651.0	.250	-.280	.520
56-33-2.03	Left	8.18	561.1	.325	-.281	.559
	Right	8.19	599.4	.329	-.281	.560
56-25-1.91	Left	8.17	542.0	.249	-.289	.519
	Right	8.17	539.6	.249	-.289	.519
33-24-1.14	Left	4.78	316.8	.235	-.291	.510
	Right	4.84	328.8	.248	-.289	.518

TABLE IV

CALCULATED UNCOUPLED FREQUENCIES OF VIBRATION

OF EXTERNAL-STORE PYLONS

Store configuration	f, cps		
	Side bending	Pitch	Yaw
56-25-3.18	170	970	35.5
56-32-2.74	170	970	38.4
56-25-2.72	170	970	39.6
56-32-2.40	170	970	41.9
56-25-2.30	170	970	45.0
56-33-2.03	170	970	47.0
56-25-1.91	170	970	51.9
33-24-1.14	222	1,260	67.5

[redacted]

TABLE V

SUMMARY OF FLUTTER CHARACTERISTICS OF TOWED MODEL

Configuration	Flutter characteristics			Wing characteristics (zero speed)			Autopilot parameters				
							Yaw		Pitch		Roll
	V_f	f_f	$\omega\bar{c}/2V$	[a] f_1	[b] f_2	f_1/f_2	K_{ψ}'	$K_{\dot{\psi}}$	K_{θ}'	$K_{\dot{\theta}}$	K_{φ}
56-25-3.18	109.5	6.45	0.209	4.21	6.27	0.671	1:1	1.06	2:1	0.495	2.0:1
56-25-3.18A	110.2	6.46	.208	4.12	6.27	.656	2:1	1.06	13:5	-----	2.6:1
56-25-3.18B	110.5	6.54	.210	----	6.29	-----	2:1	1.51	2:1	.495	2.6:1
56-25-3.18C	111.2	6.50	.208	----	-------	-----	1:1	1.06	2:1	.495	3.0:1
56-32-2.74	133.3	6.79	.181	4.24	7.05	.601	2:1	1.38	13:5	-----	2.2:1
56-25-2.72	134.5	6.88	.182	4.10	6.78	.605	2:1	1.06	13:5	-----	2.6:1
56-32-2.40	151.6	6.95	.163	4.31	7.46	.578	2:1	1.38	13:5	-----	2.2:1
56-25-2.30	158.5	6.89	.154	4.43	7.30	.606	2:1	1.38	13:5	-----	2.2:1
56-33-2.03	160.3	7.14	.158	4.28	[c] ≈7.6	≈.56	2:1	1.38	13:5	-----	2.0:1
56-25-1.91	[d] 175.3	≈7.5	-----	4.44	7.38	.602	2:1	1.38	13:5	-----	2.2:1
33-24-1.14	(e)	-----	-----	4.97	9.66	.515	1:1	1.00	2:1	.660	1.8:1
33-24-1.14A	185.9	8.56	.164	4.93	9.83	.502	1:1	1.06	2:1	.495	2.6:1
33-24-1.14B	186.6	8.48	.160	4.94	9.74	.508	1:1	1.00	2:1	.660	2.6:1
33-24-1.14C	187.9	8.46	.162	4.97	9.66	.515	1:1	0.87	2:1	.495	2.0:1
33-24-1.14D	191.0	8.48	.158	----	-------	-----	1:1	1.03	2:1	.495	2.0:1

[a] Predominantly first bending mode.

[b] Predominantly first torsion mode.

[c] Could not excite f_2 without beats due to asymmetry between left and right store inertias.

[d] Incipient flutter when model was destroyed because of autopilot power failure.

[e] Model was unflyable above 119 mph with this value of K_{φ}.

TABLE VI

FLUTTER CHARACTERISTICS OF MODEL WING

PANELS FROM FIXED-ROOT TESTS

Store configuration	Wing panel	Flutter characteristics			Wing characteristics (zero speed)				
		V_f	f_f	$\omega\bar{c}/2V$	[a] f_1	[b] f_2	f_1/f_2	g_1	g_2
56-25-3.18	Left	121.2	5.99	0.177	4.45	6.66	0.668	0.023	0.021
	Right	121.1	6.07	.180	4.46	6.51	.685	.016	.010
56-33-2.30	Right	146.0	6.39	.157	4.51	7.48	.603	.011	.025
33-24-1.14	Right	179.0	8.15	.164	5.20	9.57	.543	.024	-----

[a]Predominantly first bending mode.

[b]Predominantly first torsion mode.

[redacted]

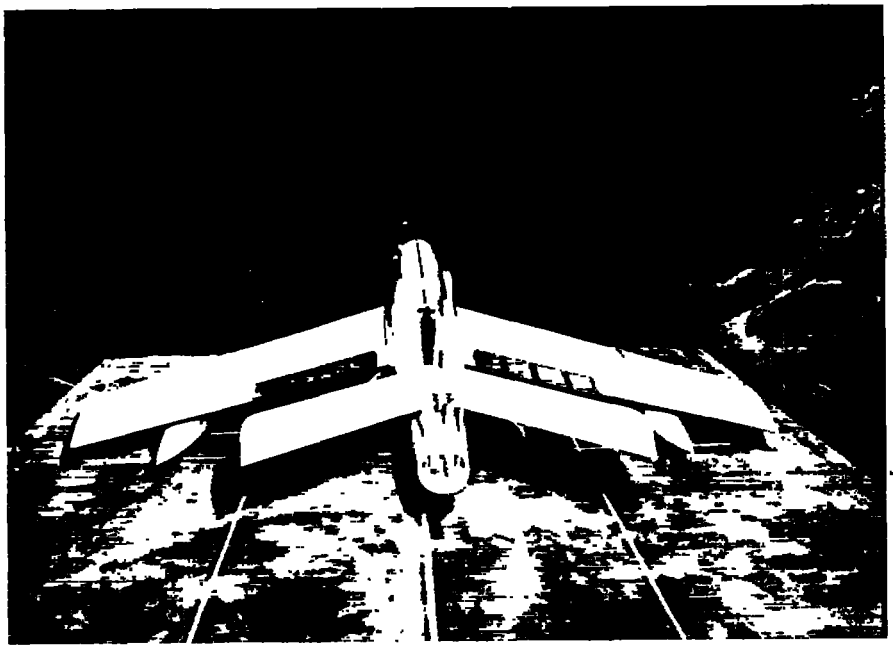

(a) Rear view.

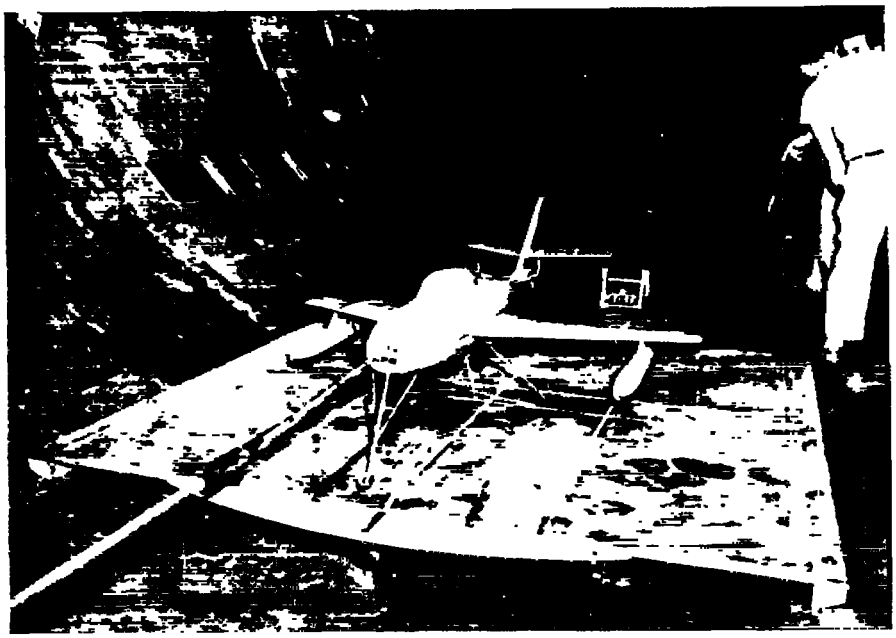

L-86463

(b) Three-quarter front view.

Figure 1.- Model resting on landing mat in the Langley 19-foot pressure tunnel.

[redacted]

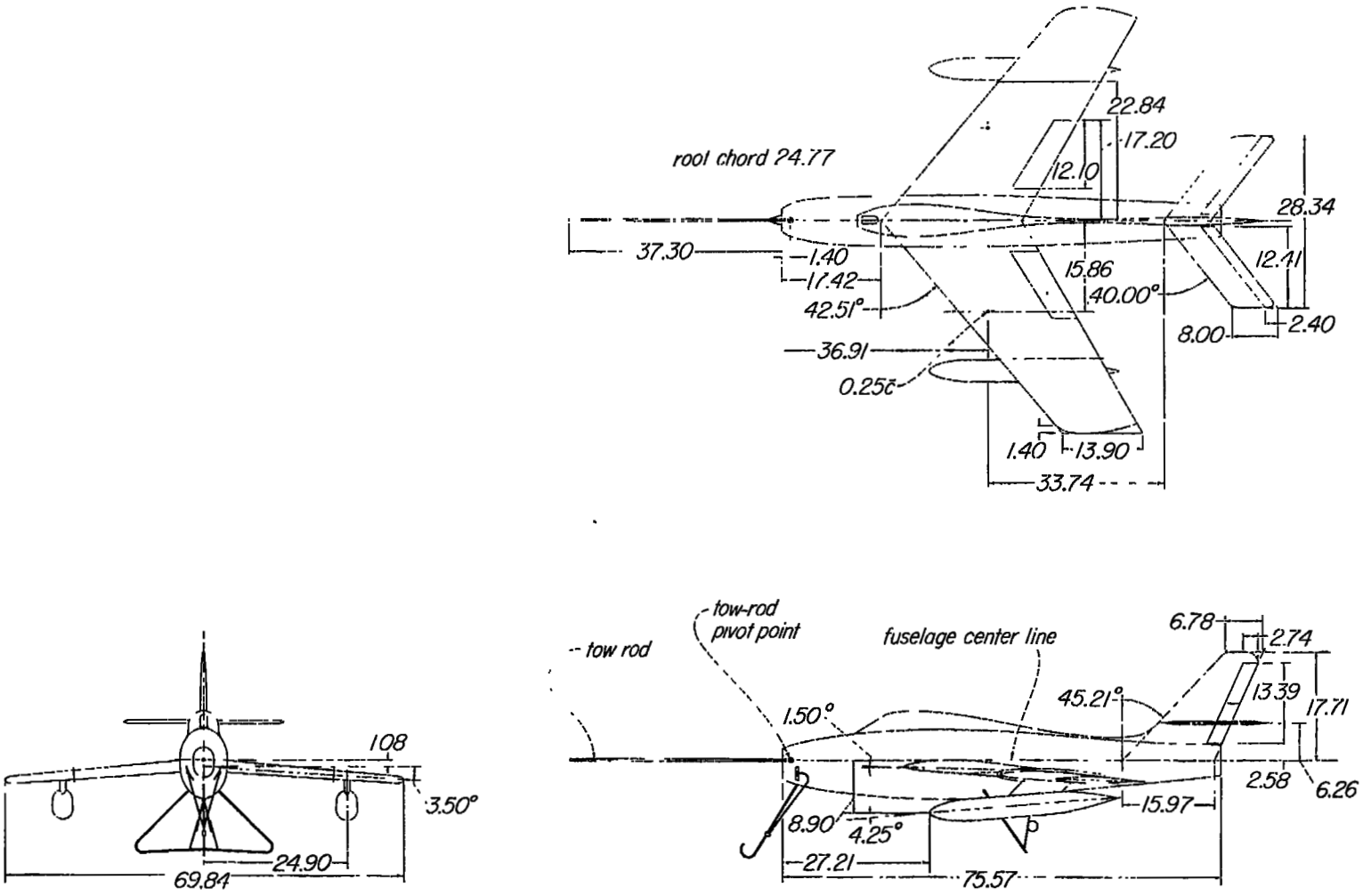

Figure 2.- Principal dimensions of the model. Wing area, 9.39 feet^2; taper ratio, 0.561; aspect ratio, 3.62; mean aerodynamic chord, 19.84. All dimensions are in inches unless otherwise noted.

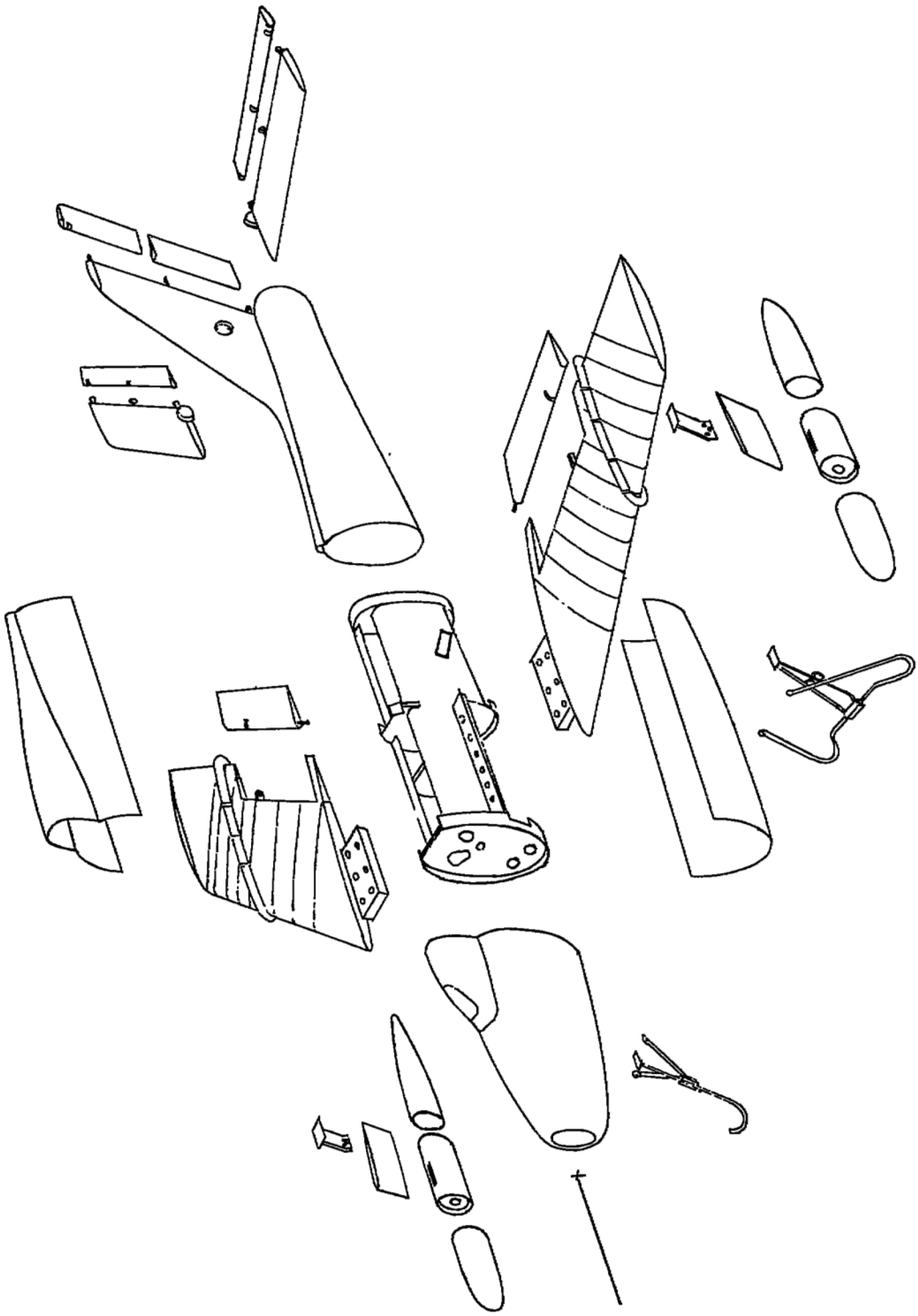

Figure 3.- Model structural components.

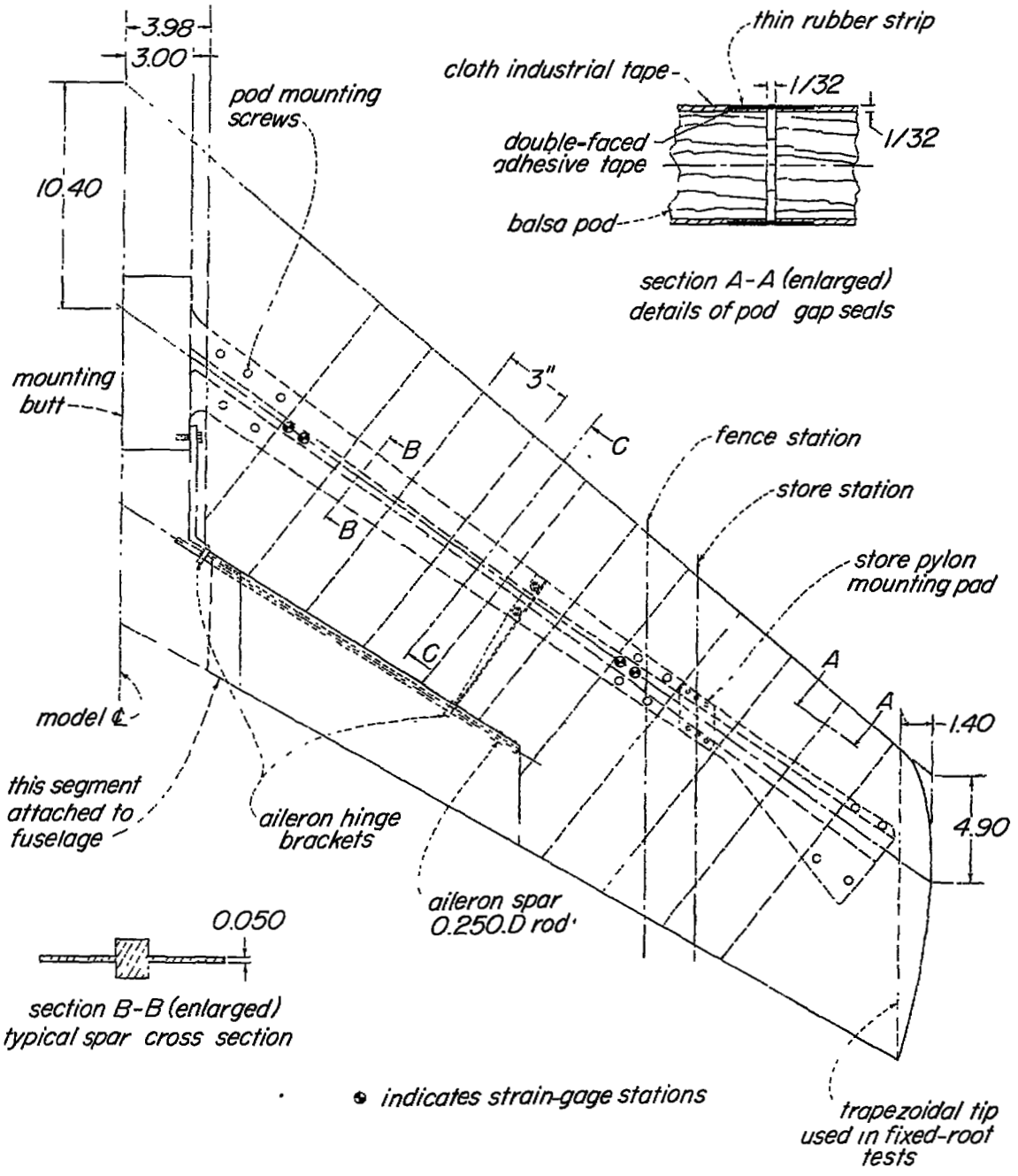

(a) Overall assembly. Approximate weight, 16.75 pounds.

Figure 4.- Construction details of model wing panels. All dimensions are in inches.

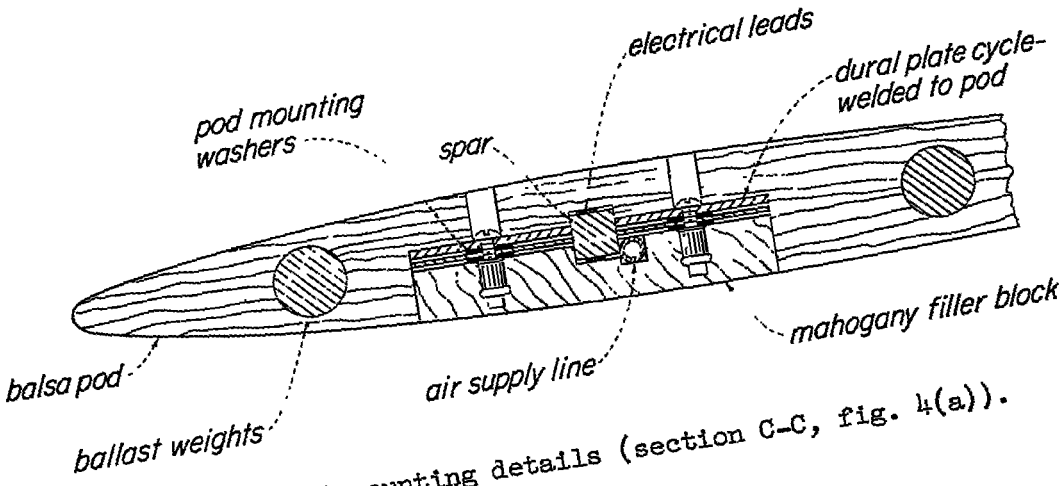

(b) Wing-pod mounting details (section C-C, fig. 4(a)).

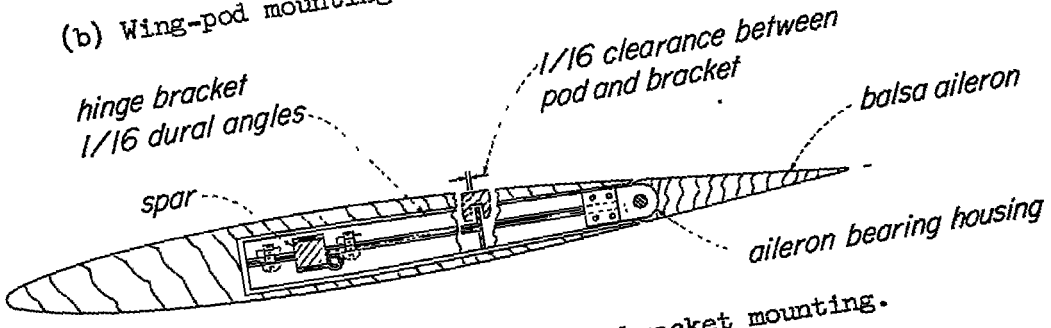

(c) Outboard aileron hinge bracket mounting.

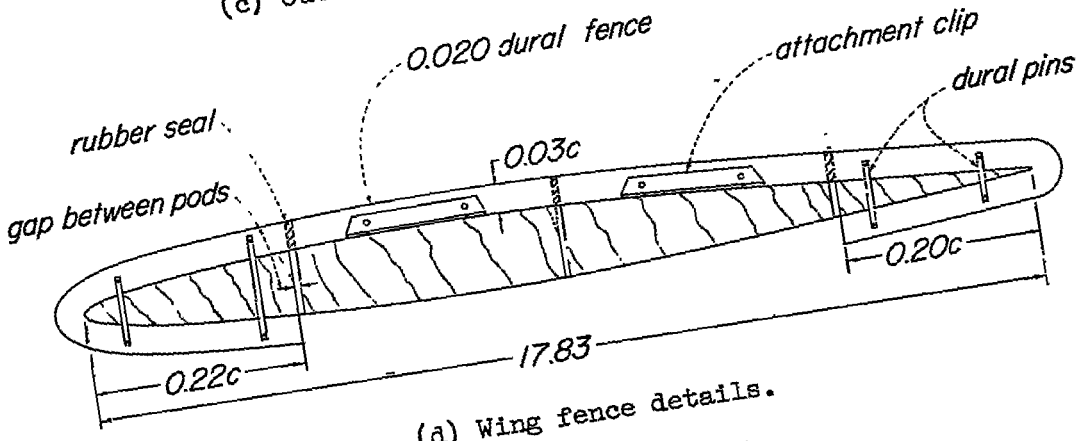

(d) Wing fence details.

Figure 4.- Concluded.

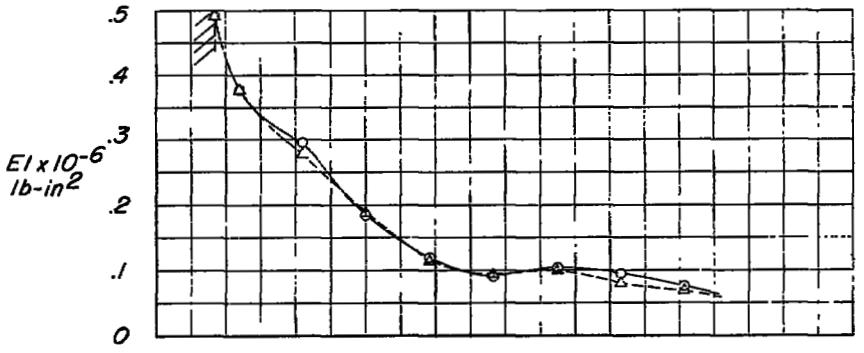

(a) Bending rigidity.

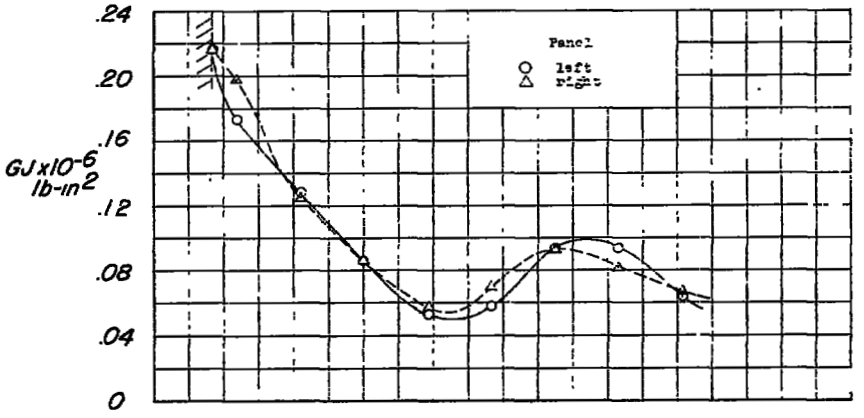

(b) Torsional rigidity.

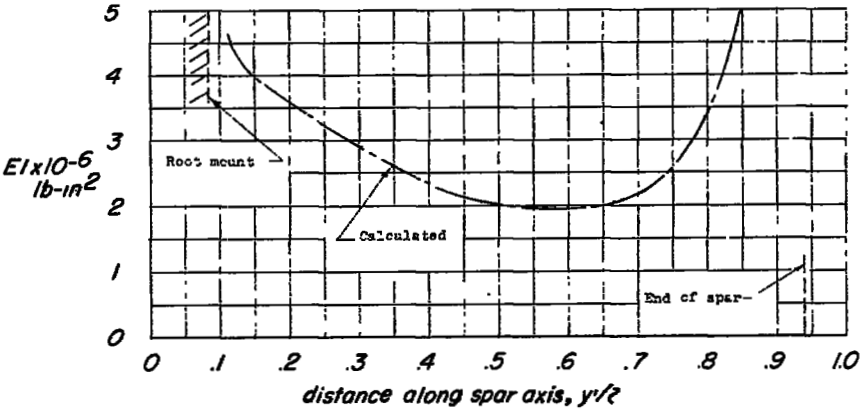

(c) Drag rigidity.

Figure 5.- Structural characteristics of model wing panels.

[redacted]

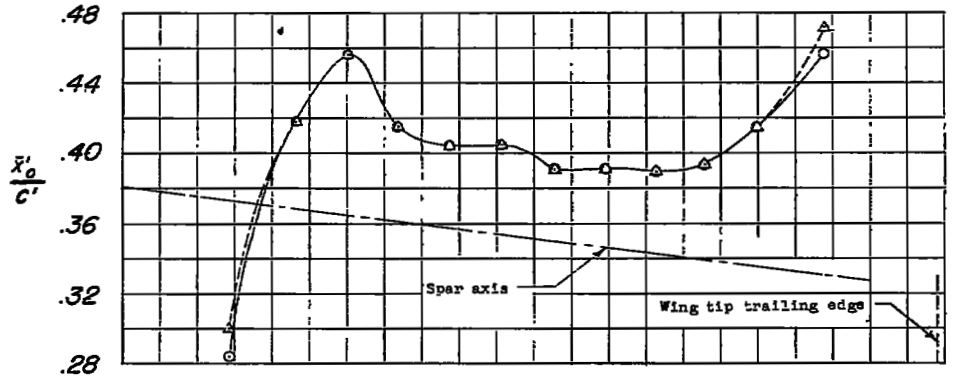

(a) Section centers of gravity and spar axis locations.

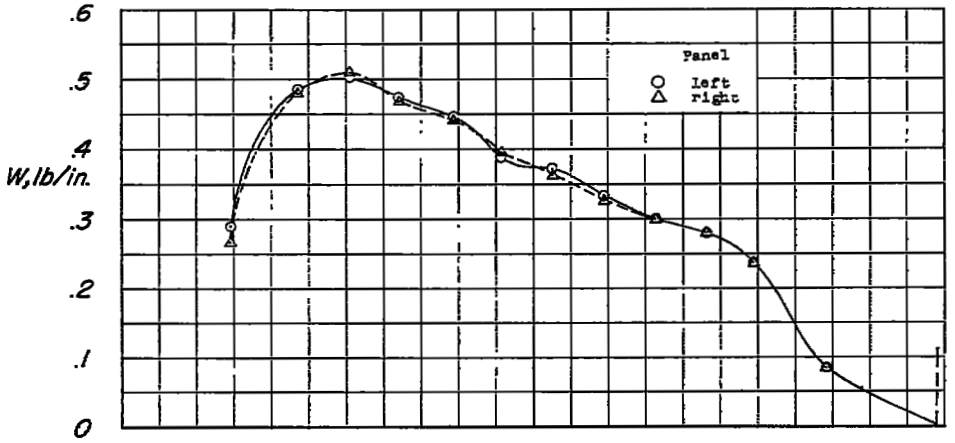

(b) Weight distribution.

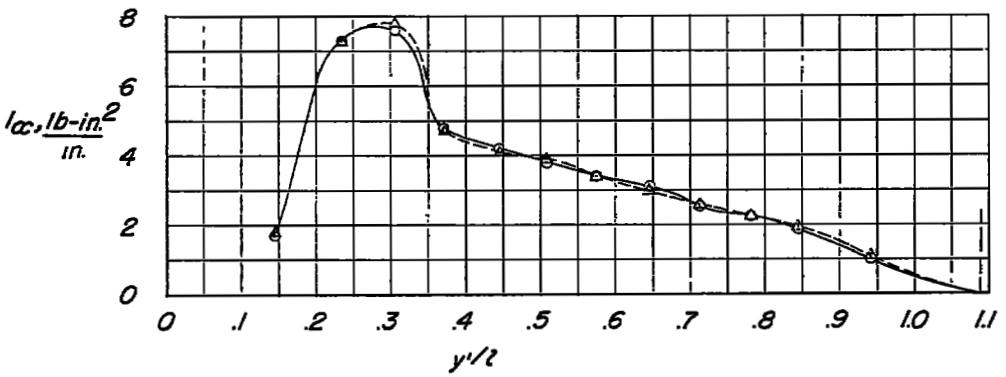

(c) Section weight moments of inertia about spar axis.

Figure 6.- Mass parameters of model wing panels.

[redacted]

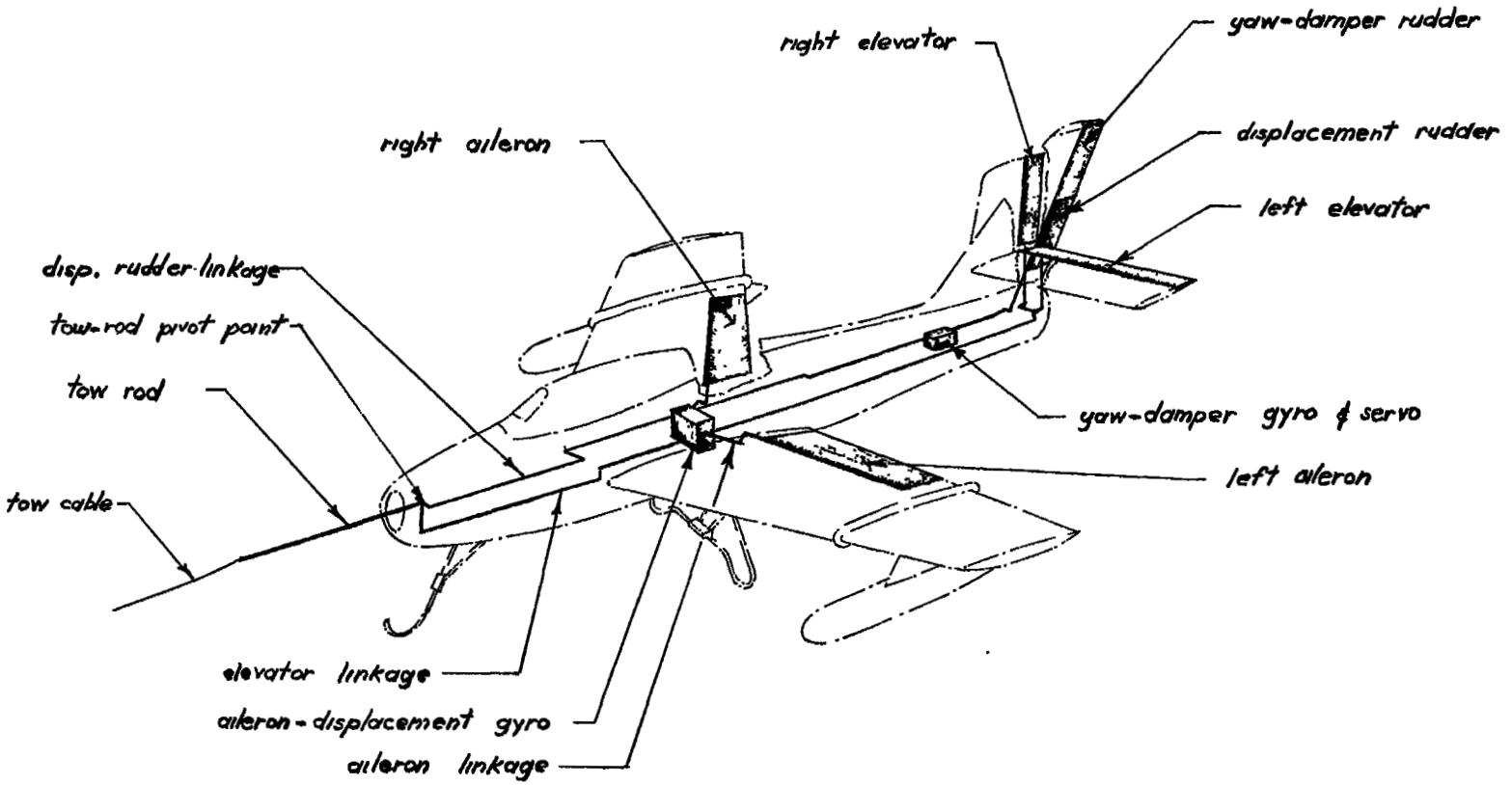

Figure 7.- Model control system.

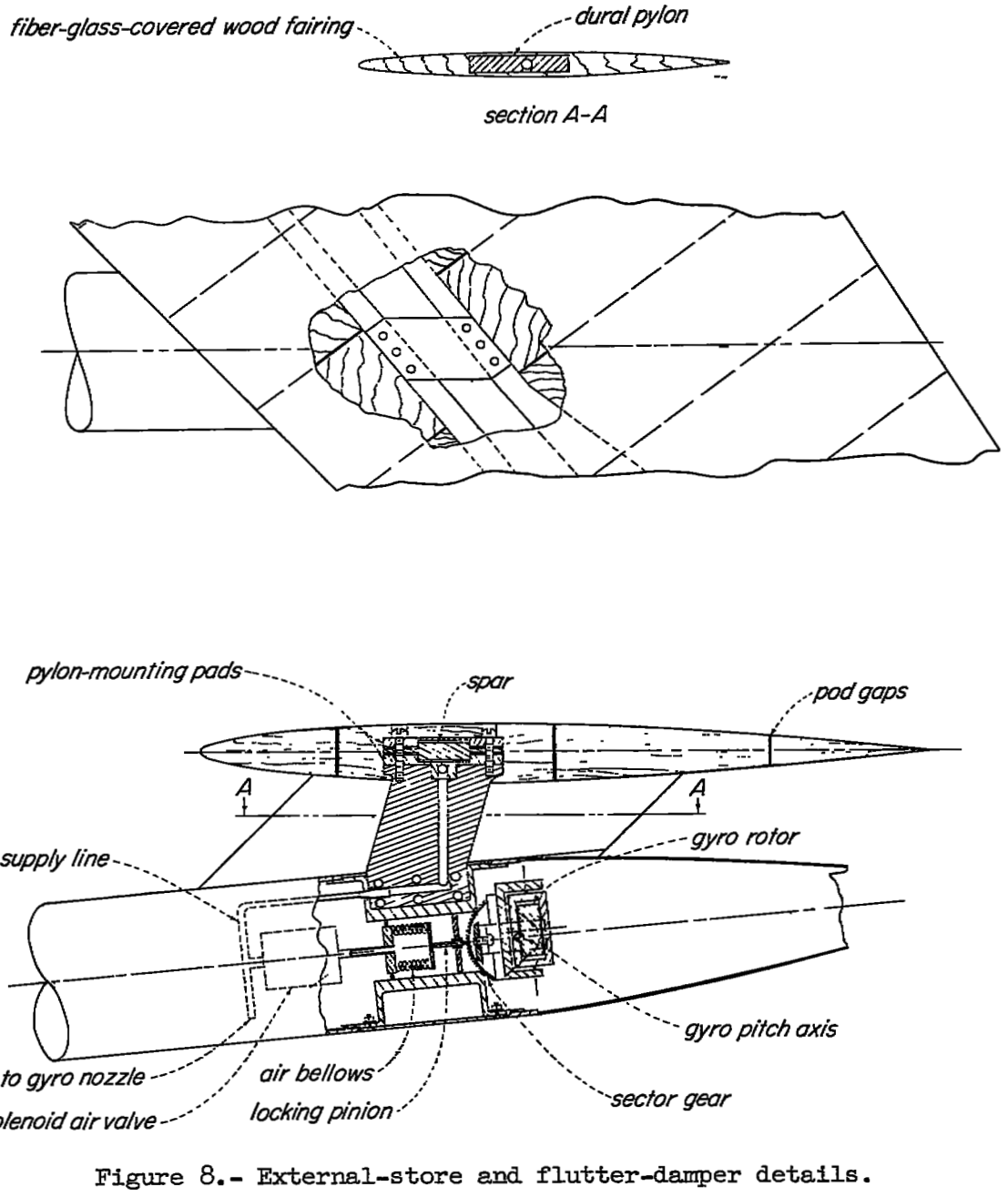

Figure 8.- External-store and flutter-damper details.

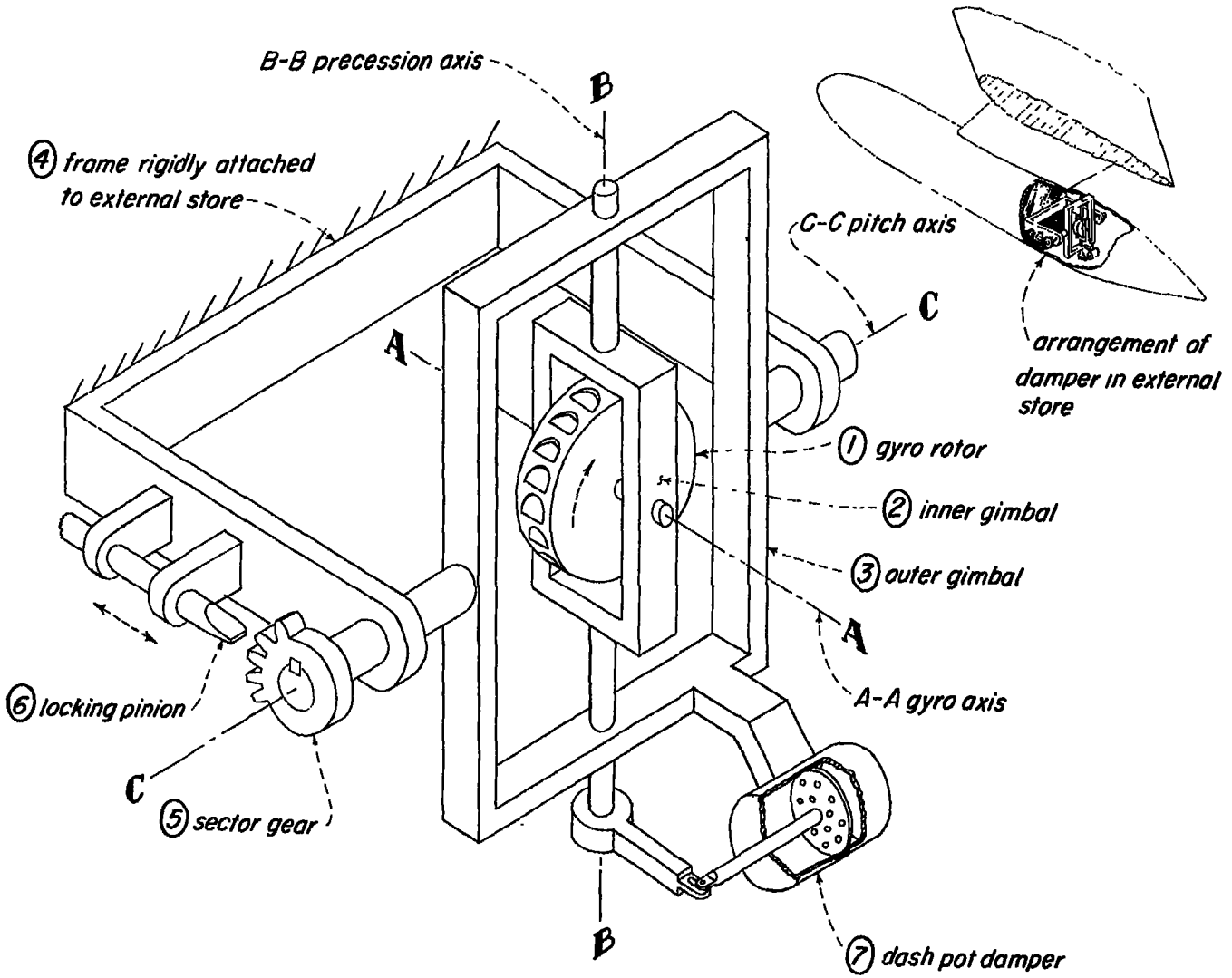

Figure 9.- Schematic arrangement of model flutter damper.

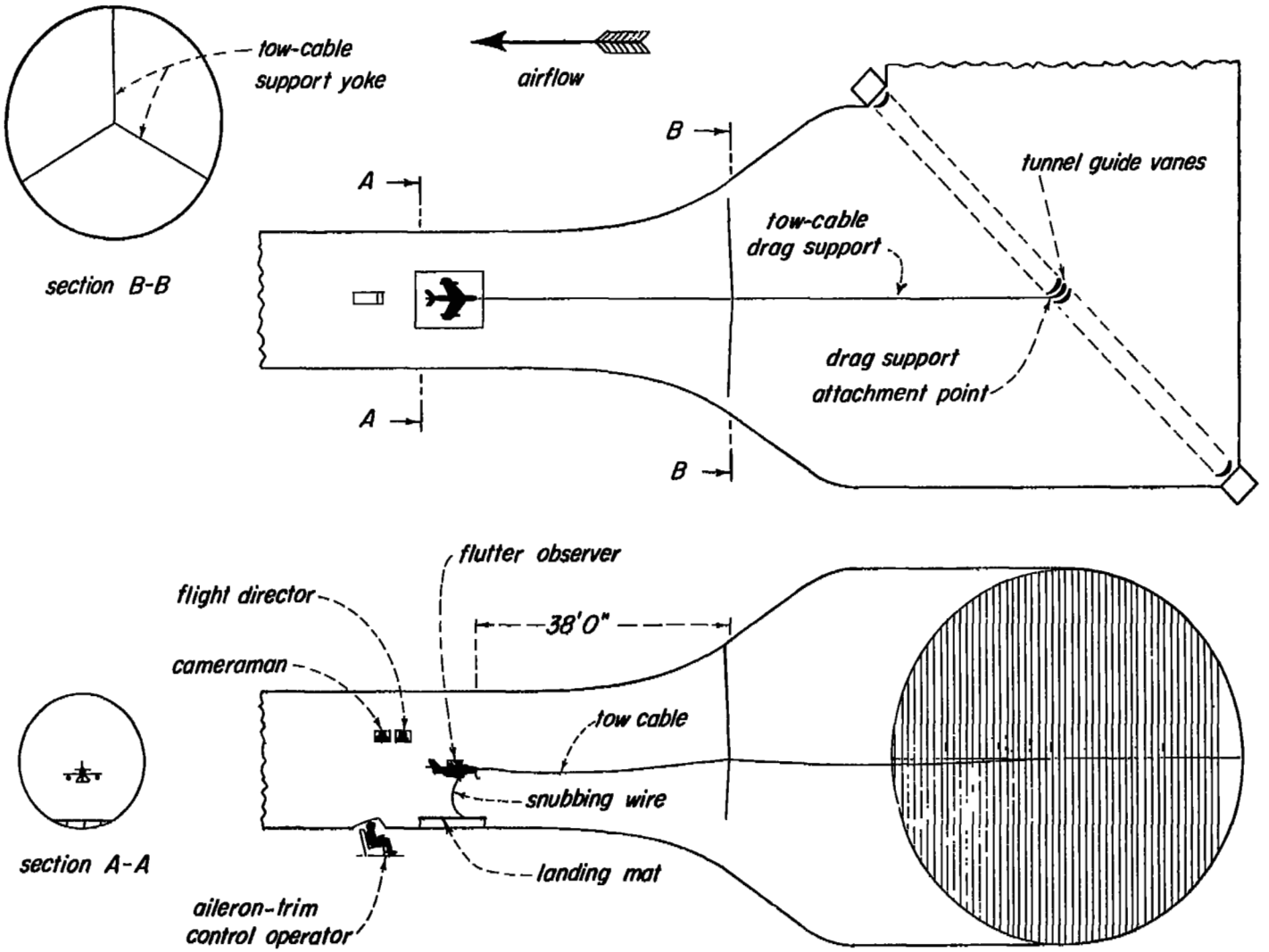

Figure 10.- The towed-model test arrangement in the Langley 19-foot pressure tunnel.

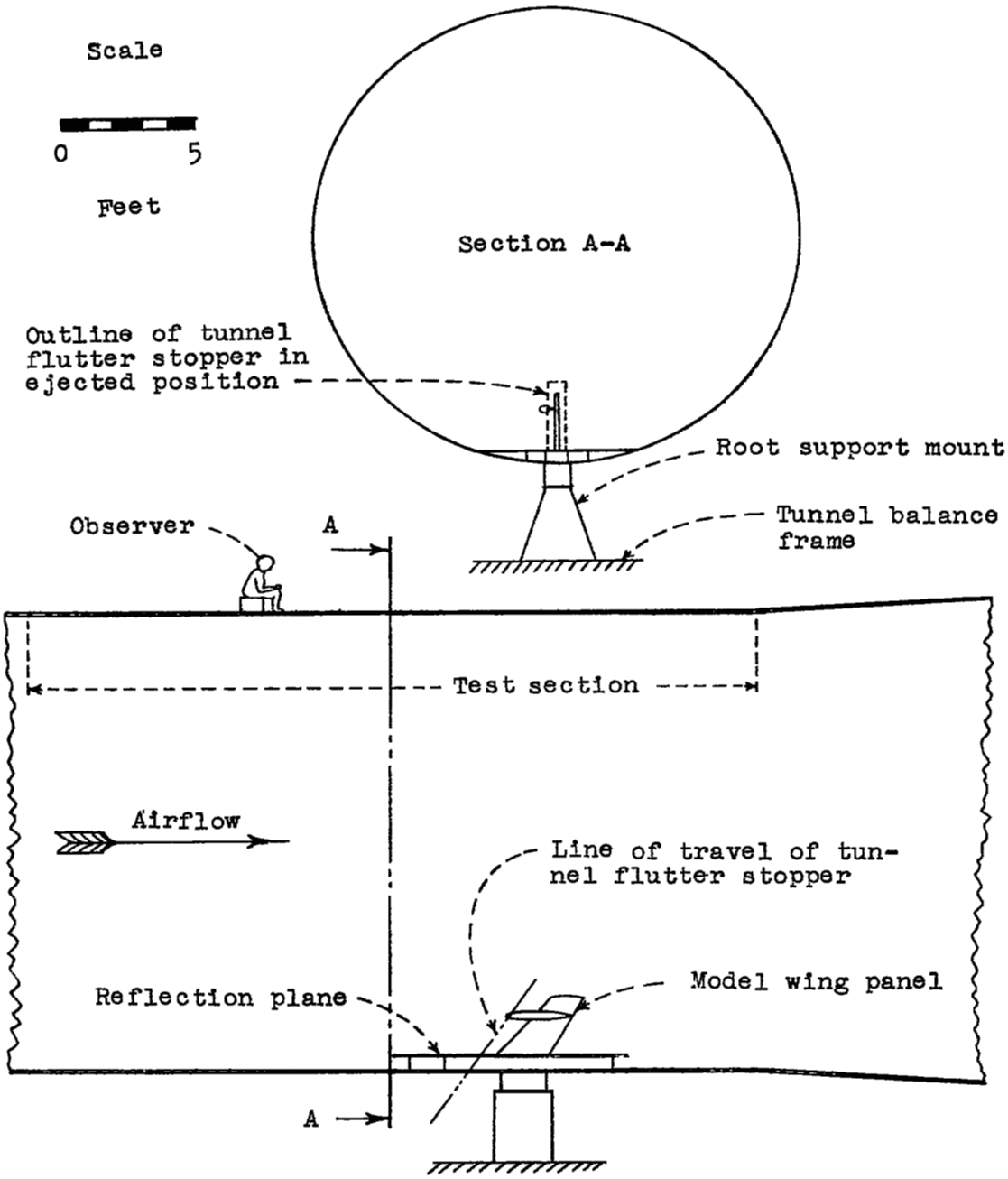

Figure 11.- Fixed-root flutter-test setup in the Langley 19-foot pressure tunnel.

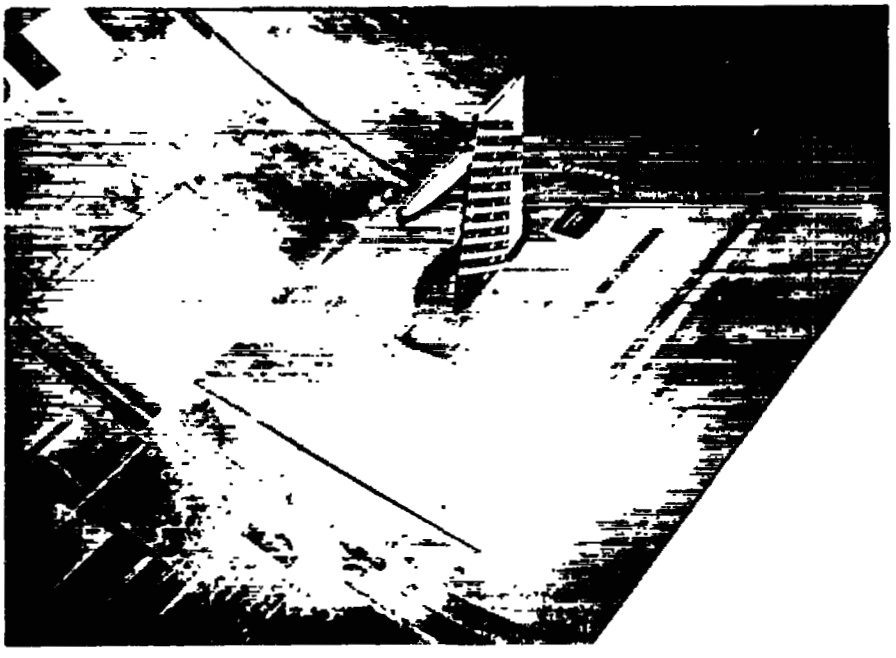

(a) Overall view of reflection plane and model wing panel.

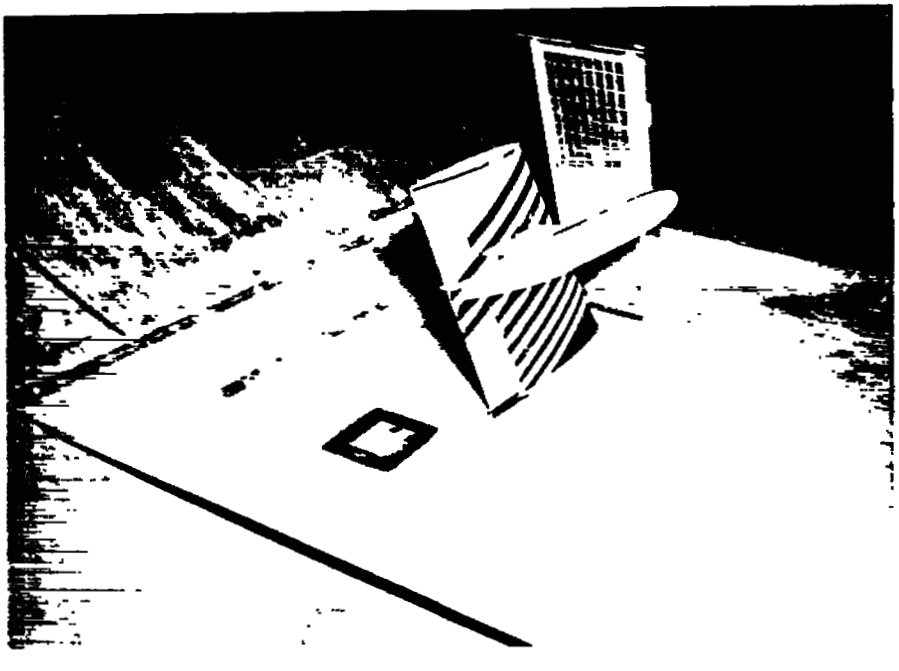

L-86464

(b) Model wing panel with tunnel flutter stopper in ejected position.

Figure 12.- Fixed-root flutter-test setup of right wing-panel—store combination.

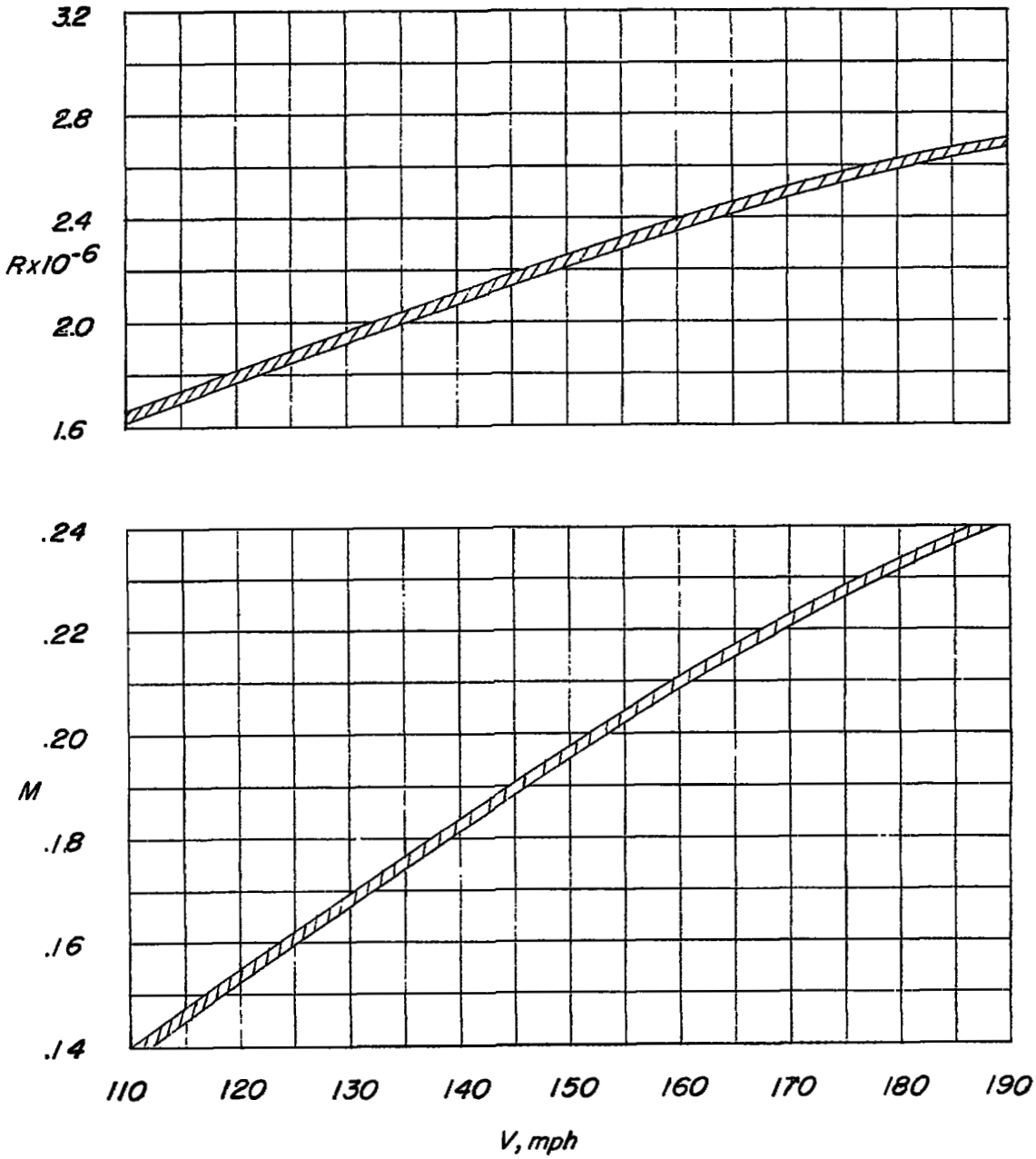

Figure 13.- Reynolds number and Mach number variations of tests.

[redacted]

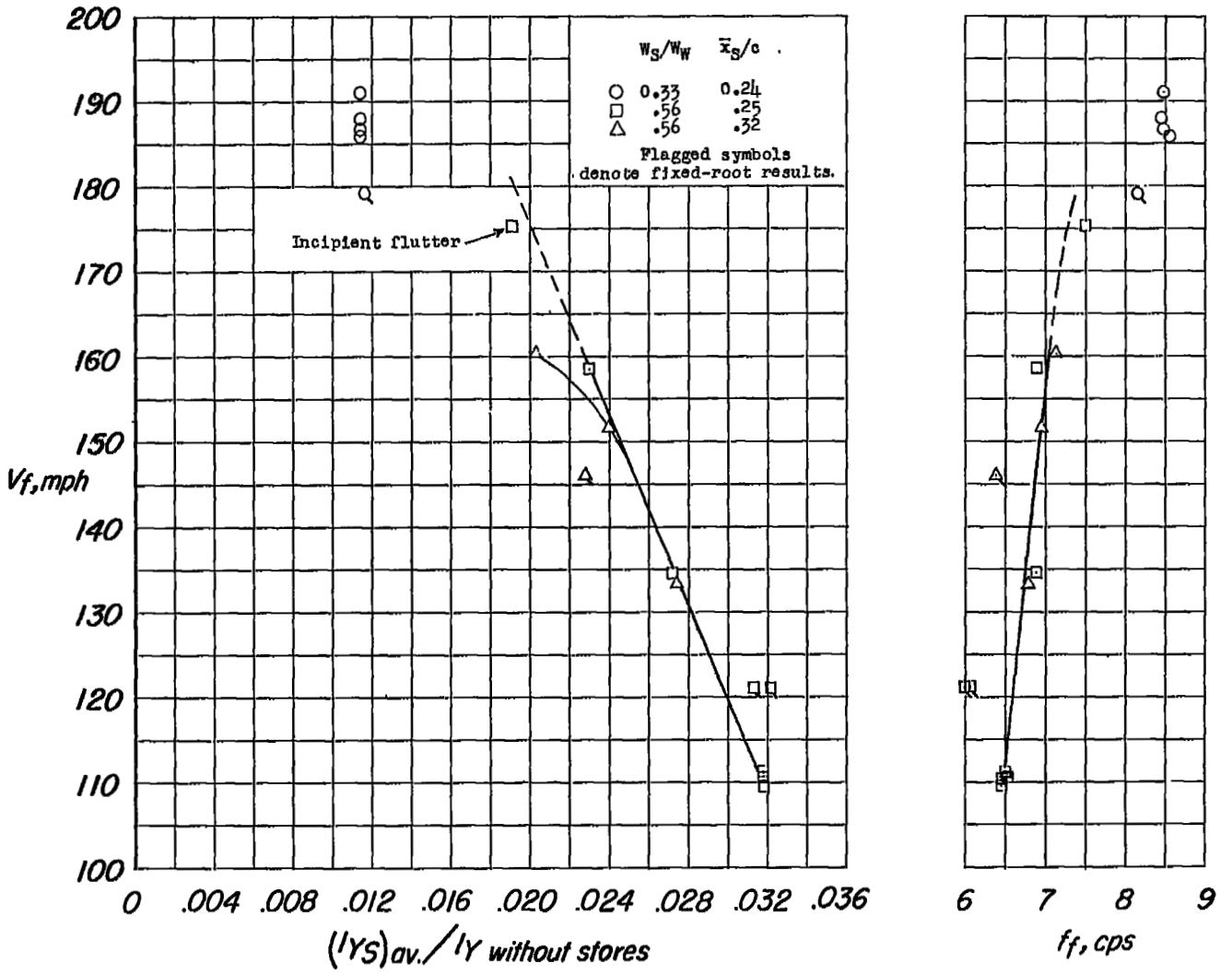

Figure 14.- Flutter characteristics of towed model and comparison with the fixed-root characteristics.

Channel Trace		Sense*
1.	Reference	
2.	Accelerometer 2 inches right of center of gravity	
3.	Right flutter damper	
4.	Accelerometer 6 inches aft of center of gravity	
5.	Accelerometer at center of gravity	
6.	Displaced rudder position	
7.	Right outboard bending	down
8.	Right outboard torsion	up
9.	Left outboard torsion	down
10.	Left outboard bending	down
11.	Canopy light	
12.	Right inboard torsion	down
13.	Right inboard bending	down
14.	Left flutter damper	
15.	Left inboard torsion	up
16.	Left inboard bending	down
17.	Yaw damper position	
18.	Aileron position	
19.	Elevator position	
20.	Reference	

*Indicates directions of downward bending and increased angle of attack.

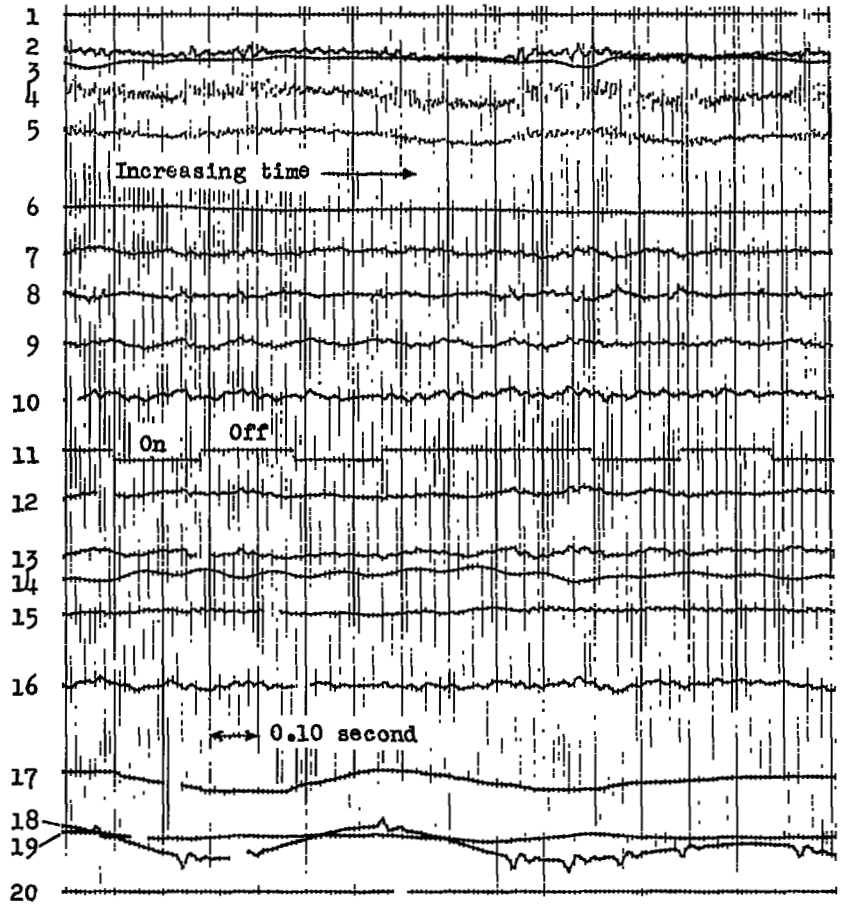

(a) $0.955V_f$.

Figure 15.- Portions of oscillograms made during a typical flutter test of the towed model. Channel sensitivities between accelerometer traces and between the left- and right-wing gage traces are not identical.

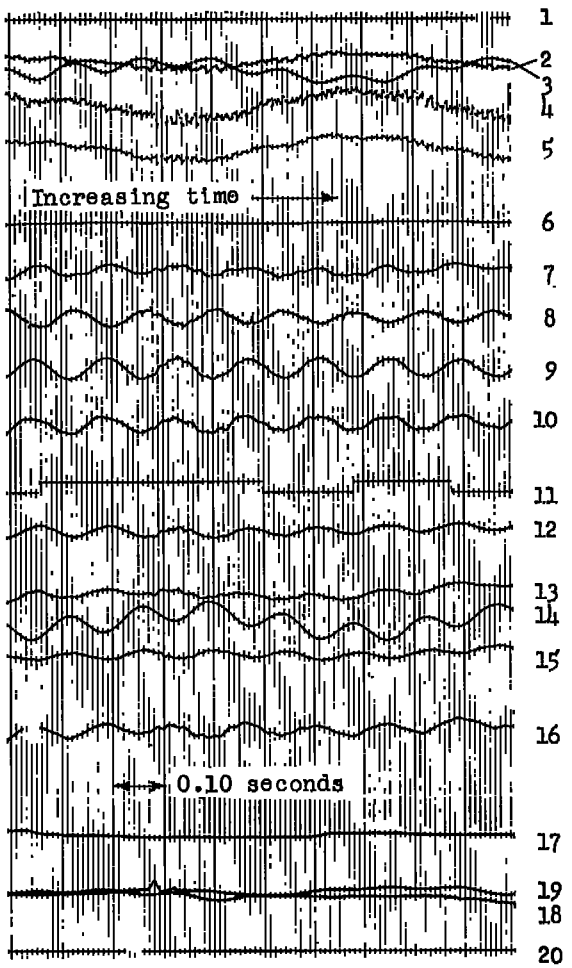

(b) $0.978V_f$.

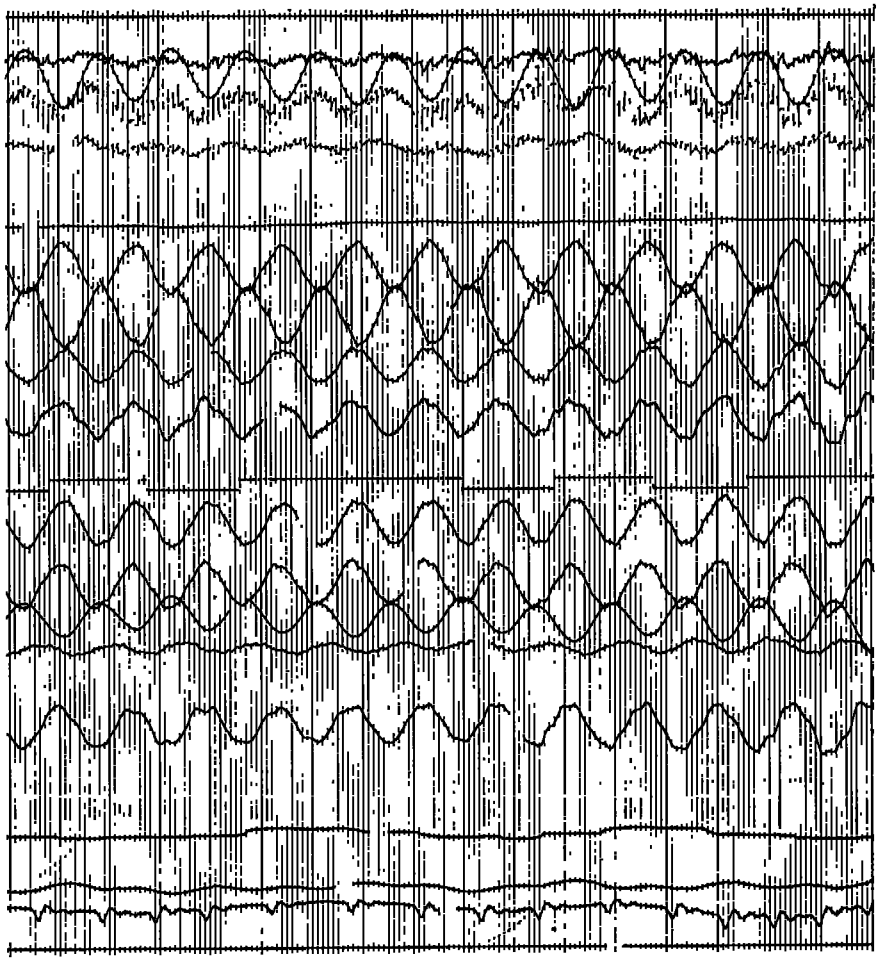

(c) V_f.

Figure 15.- Concluded.

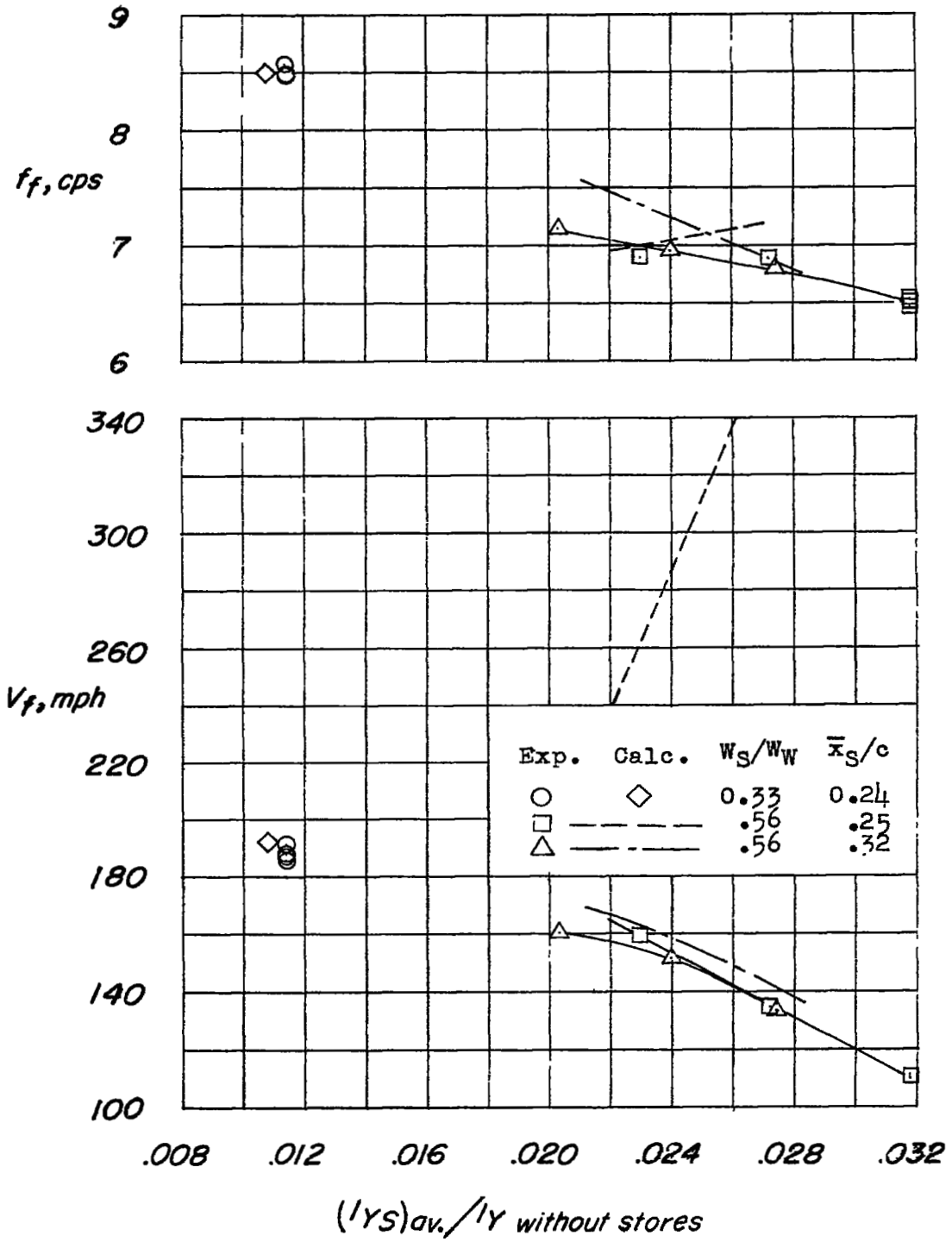

Figure 16.- Experimental and calculated flutter characteristics of towed model.

[redacted]

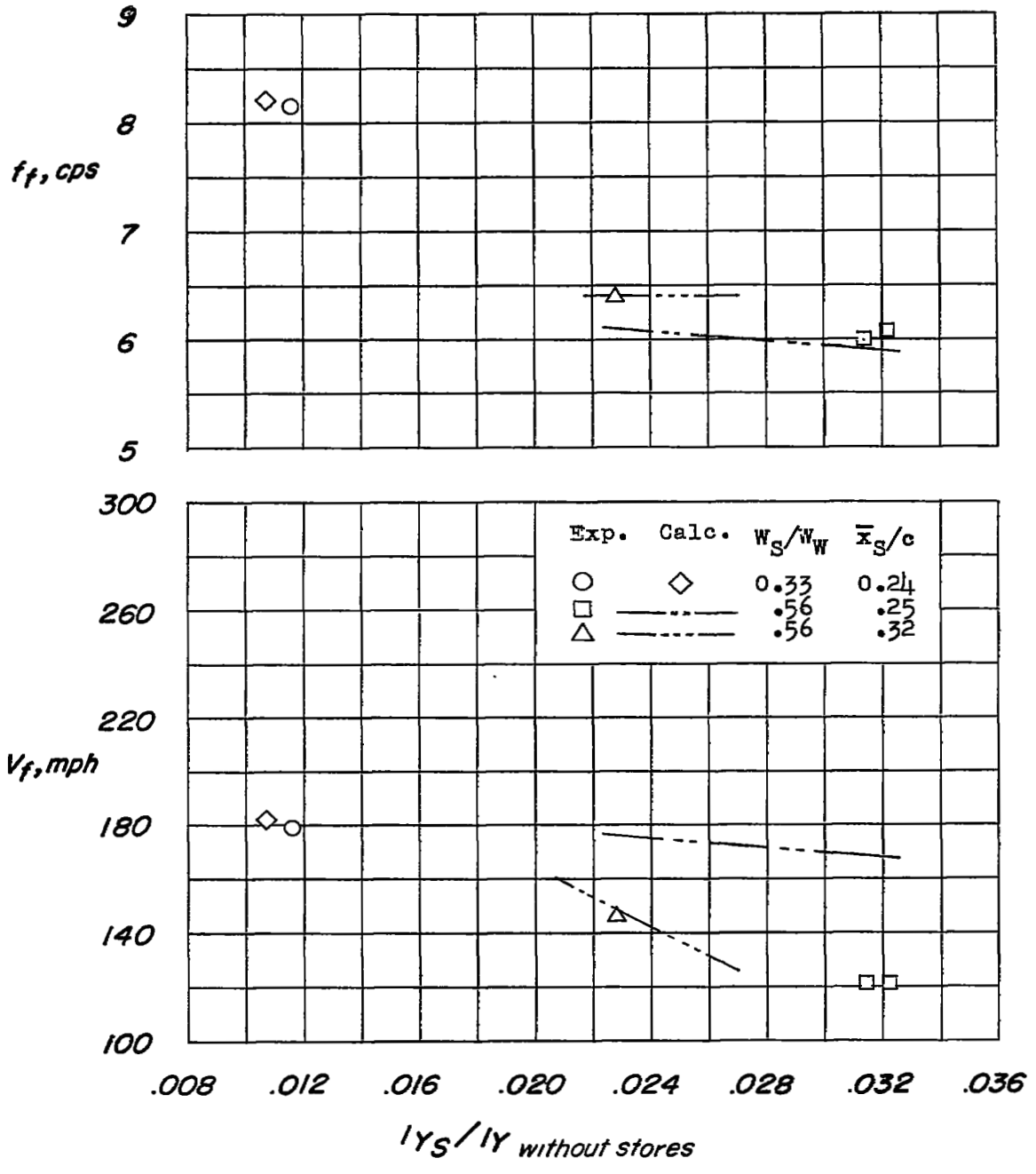

Figure 17.- Experimental and calculated flutter characteristics of model wing panels with root fixed.